Compressive strength of collar plate reinforced SHS T-joints: Effect of geometrical parameters and chord stress ratio

Compressive strength of collar plate reinforced SHS T-joints: effect of geometrical parameters and chord stress ratio

Hongfei Chang[1,2*], Wenkang Zuo[1], Jianchao Yang[1], Xinyi Song[1], Yuner Huang[3]

[1]*JiangSu Key Laboratory of Environmental Impact and Structural Safety in Engineering, China University of Mining and Technology, Xuzhou, China*

[2]*State key Laboratory of Geomechanics and Deep Underground Engineering, China University of Mining and Technology, Xuzhou, China*

[3]*School of Engineering, University of Edinburgh, Edinburgh, Scotland, UK*

[*]*(Corresponding author: E-mail: honfee@126.com)*

Highlights:

(1) Effect of geometrical parameters and chord stress on the compressive strength of CPR SHS T-joint is investigated;

(2) Typical failure modes of the CPR SHS T-joints under compressive load are identified;

(3) Design equations are established to determine the compressive strength of CPR SHS T-joints.

Abstract

The collar plate (CP) is applicable for the reinforcement of both new designed and in-service joints, yet the design approach for the reinforcement requires further investigation. The current paper investigates the effect of various geometrical parameters as well as chord stress ratios on the compressive capacity of the collar plate reinforced (CPR) square hollow section (SHS) T-joints. The finite element (FE) models of the CPR SHS T-joints are built and validated using experimental data. Extensive parametric studies are carried out to evaluate the influence of parameters such as the brace to chord width ratio, the width/length and thickness of the CP, as well as the chord stress ratio. The brace to chord width ratio and the CP thickness are identified as the key parameters, and three typical failure modes are observed. Finally, bearing mechanism of CPR T-joints is discussed and design equations are proposed based on the failure modes. The failure-mode-based equations agree well with both parametric data and orthogonal analysis results, which provides reference for the practicing engineers.

Keywords: compressive strength; collar plate; reinforced SHS T-joint; parametric study; chord stress ratio; finite element analyses.

Notations

b_0	Chord width	$\overline{N_u^R}$	Normalized ultimate strength of reinforced joint
b_1	Brace width	$\overline{N_u^{UR}}$	Normalized ultimate strength of unreinforced joint
b_2	Collar-plate width	Q_f	Function for the chord stress
E	Elastic modulus	Q_u	Normalized compressive strength
f_{u0}	Ultimate stress of chord member	S_e	Reinforcement efficiency
f_{u1}	Ultimate stress of brace member	t_0	Chord wall thickness
f_{u2}	Ultimate stress of collar-plate	t_1	Brace wall thickness
f_{y0}	Yield stress of chord member	t_2	Collar-plate thickness
f_{y1}	Yield stress of brace member	β	Brace to chord width ratio (b_1/b_0)
f_{y2}	Yield stress of collar-plate	N_0	Chord end load
h_0	Chord height	2γ	Chord width to thickness ratio(b_0/t_0)
h_1	Brace height	γ_2	Collar-plate length to chord width ratio(L_2/b_0)
L_0	Chord length	τ_2	Collar-plate to chord thicknesses ratio (t_2/t_0)
L_1	Brace length	η	Brace height to chord width ratio (h_1/b_0)
L_2	Collar-plate length	η_2	Collar-plate length to chord width ratio (L_2/b_0)
n	Chord end pre-load ratio	χ	Reduction factor for flexural buckling
		ε_y	Strain at yield stress
		ε_u	Strain at ultimate stress

N	Actual axial load on the brace	δ	Actual axial brace displacement
$\overline{N_0}$	Normalized load on the brace	$\overline{\delta_0}$	Normalized brace displacement
$\overline{N_u}$	Normalized ultimate strength of the joint		

1. Introduction

Tubular joints of square hollow section (SHS) are widely adopted in large span structures [1]. Local reinforcement has been proved effective to increase both the strength and the stiffness of the SHS joints, and thus the implementation of reinforced SHS tubular joints becomes increasing popular in practices [2,3]. However, the effect of geometrical parameters and chord stress ratio on reinforced joints is unclear, and the design approach for the reinforced joints still requires further investigation.

For the reinforcement of SHS joints, the external methods such as welding plates[4-6] or ring stiffeners[7,8], as well as gluing FRP sheets[9,10] have been widely used as they are convenient to be implemented. Amongst these methods, doubler plate[4,11,12] and collar plate[6,11,12] are preferred by the designers, since they have least impingement on the architectural appearance. However, the doubler plate and collar plate is only effective to reinforce the flange of the chord and thus is more advisable for SHS joints failure by chord flange yielding. For SHS joints failure by the buckling of the chord web, the sidewall plate[13] or L-shaped collar-plate[14] reinforcement is more suitable. The configurations of typical external plate reinforcements are shown in Fig. 1. It can be seen the doubler plate is only applicable for new designed joints, while the collar plate is applicable for both new designed and in-service joints[15] which bring more feasible applications of collar plate reinforcement method.

As to the reinforcement performance of the collar plate, it has been proved effective to enhance the strength of both circular hollow section (CHS) and SHS joints. The test by Choo et al. [16] indicated that the collar plate reinforced CHS T-joint even shows better compressive strength than the doubler plate reinforced (DPR) ones. The numerical results by Nassiraei et al. [17] shown a maximum enhancement of 270% in compressive capacity by the collar plate reinforcement on CHS T/Y joints. Shao [18] investigated the structural performance of collar plate reinforced CHS T-joints under static load, and found the enhancement on compressive capacity is up to 22.6%. The enhancement of collar plate on strength for SHS joints is also apparent[12,19,20], for example the tested enhancement ratios of compressive strength by Ozyurt et al.[19] and Feng et al.[20] are 83.6% and 123%, respectively. The difference of the enhancement ratio mainly comes from two aspects, namely the brace to chord width ratio (β) and the dimensions of the collar plate[16, 18]. For example, the brace to chord width ratios of tests by Shao[18] are 0.25 to 0.69, comparing to 0.5 by Ozyurt et al.[19], and 0.53, 0.67 and 0.8 by Feng et al.[20]. The thickness ratios of the collar plate to the chord (τ_2) varied from 1.0 to 1.5 in the tests [12,19,20]. Amongst the above tests, the yielding of chord flange or collar plate was found to be the control failure mode for most of the CPR SHS specimens. However, further parametric studies also observed the failure of chord web buckling, especially for CPR SHS joints with a high β and τ_2 ratio[19,20]. This is mainly due to the "over-reinforcement" effect of the collar plate for the chord flange, which has also been observed for DPR SHS T-joints[21,22]. Although both the above failure modes have been observed for CPR SHS joints under compressive load, their identification criteria is not yet clear, which brings uncertainties for the prediction of the joint strength.

Up to now, the design equations for the DPR or CPR SHS joints have also been investigated widely, and some of them are quoted in Table 1. It is shown that more attentions have been paid on DPR SHS joints than that of CPR ones, and a thick doubler plate is suggested by EC3[23] and CIDECT[24]. This is reasonable for joints under in-plane bending or tension, since a thick doubler plate is essential to guarantee a tight contact between the plate and the chord flange. While for SHS joints

under compressive load, it is shown to be uneconomic to use a thick doubler plate [22]. Therefore, revisions have been done by Ozyurt et al. [19], Feng et al.[20], Chang et al. [21] and Lima et al. [22] to reduce the thickness of the doubler plate. For the compressive strength design of CPR SHS joints, the equations for DPR joints by EC3[23] and CIDECT[24] were found un-conservative and unsafe in some cases[19]. Ozyurt et al.[19] and Feng et al.[20] have introduced a modify coefficient to consider the enhancement of collar plate on the strength of chord flange yielding. Their equations are similar in expressions, and have been proved reliable to predict the compressive strength of CPR SHS joints. However, the change of failure modes has not been taken into account in these empirical equations, and thus further attentions need to be paid on the design of reinforced SHS joints based on failure modes.

Another issue on the behavior of reinforced SHS joint is the influence of chord stress ratio. In the current guidelines of EC3[23] and CIDECT[24], the chord stress function (CSF) of Q_f is adopted to account for the negative influence of chord stress on unreinforced SHS joints. Liu et al. [26] proposed a general form of CSFs, which seems controversial due to the differences of boundary conditions and joint dimensions. The analysis by Garifullin et al. [27] indicated that the existing CSFs for resistance are inapplicable for initial stiffness, and thus proposed new functions for initial stiffness. Similarly, the applicability of the existing CSFs for reinforced joints is also unclear. Qu et al. [28] have tested the dynamic performance of CPR CHS T-joints with chord pre-compression, by which they found the presence of collar plate improves the impact resistance of the joint significantly. However, they did not discuss the influence of chord stress level. Recently, Chen et al. [29] reported their experimental and numerical analysis on CHS X-joints reinforced with external ring stiffeners and gusset plates. The results indicated that the stiffeners may change the effect of chord stress on the joint behavior, the existing CSFs for unreinforced joints are conservative for reinforced ones, and then new CSFs were proposed. The preliminary analysis by the authors[14] also indicated that the influence of chord stress on reinforced SHS joint is different from that of unreinforced ones.

This paper presents an investigation on the influences of various geometrical parameters as well as chord stress ratios on the compressive capacity of the CPR SHS T-joints. Extensive parametric study has been carried out with finite element models that validated against experimental data. Typical failure modes and failure criteria are identified, and corresponding design equations are proposed. The study shows that the failure-mode-based design equations are reliable and accurate to predict the compressive strength of CPR SHS T-joints, which can provide reference for the practicing engineers.

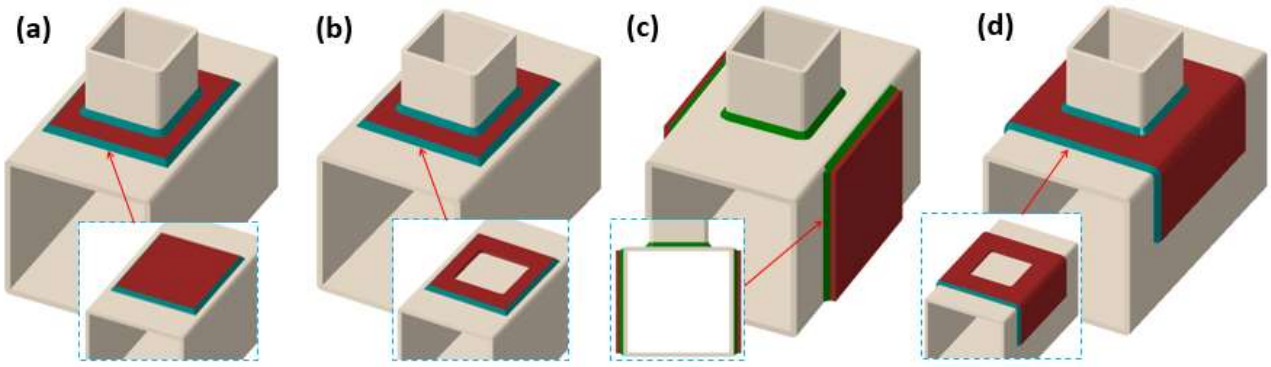

Fig. 1. Typical chord surface welding plate reinforcement methods. (a) DPR SHS T-joint, (b) CPR SHS T-joint, (c) Sidewall plate reinforcement, (d) L-shaped CPR SHS T-joint.

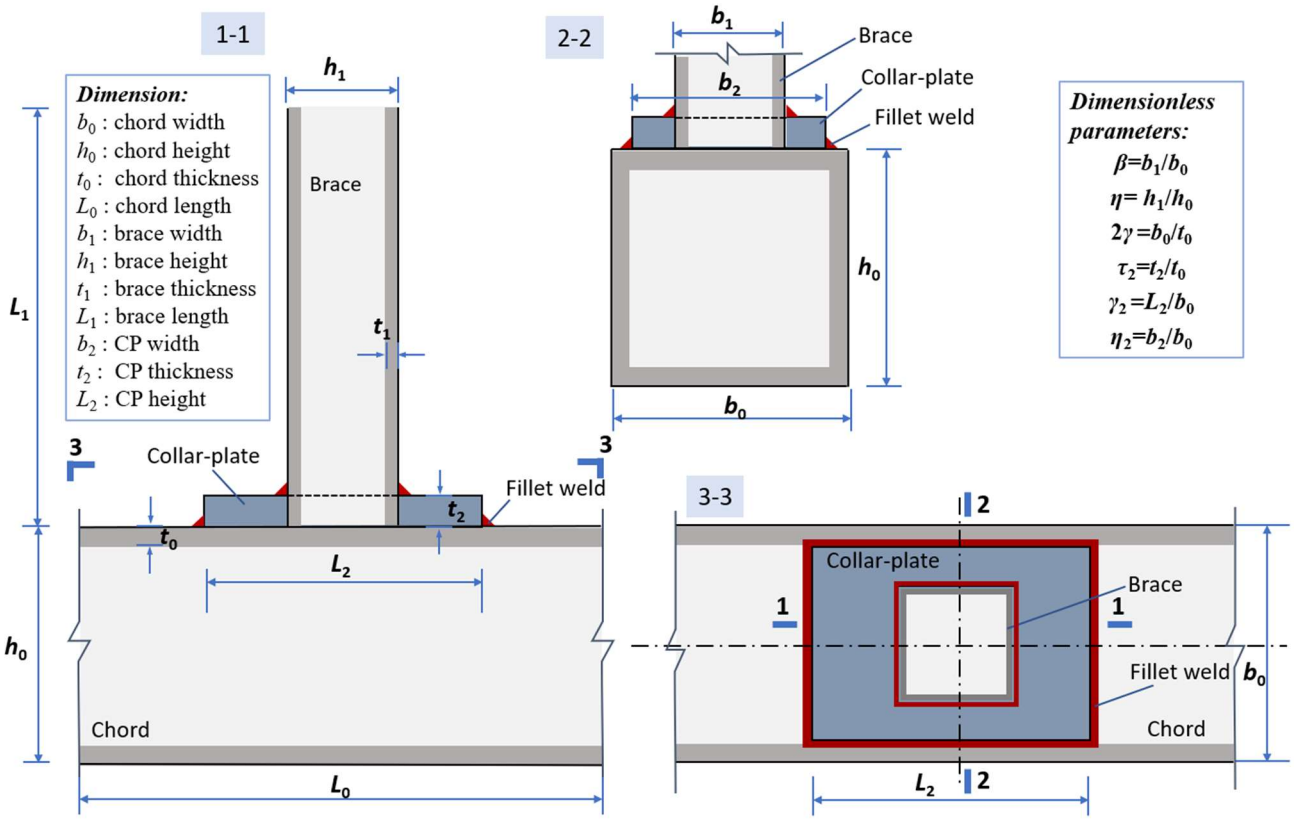

Fig. 2. Geometrical parameters of collar plate reinforced SHS T-joint

Table 1 Design resistances of DP or CP reinforced SHS T-joint under brace compression

Reference	Type	Application range				Design equation
		$\beta=b_1/b_0$	$\tau_2=t_2/t_0$	$\gamma_2=h_2/b_0$	$\eta_2=b_2/b_0$	
Ozyurt[19]	DPRT CPRT	[0.3, 0.75]	[1, 3]	$\geq\eta+\sqrt{\eta_2(\eta_2-\beta)}$	$\geq 1-2t_0/b_0$	$Q_f Q_u f_{y0} t_0^2 \psi_1$ $\psi_1 = 3.227 - 3.143\beta + 0.121\tau_2$
Feng [20]	DPRT CPRT	[0.3, 0.85]	[1, 2.5]	-	[1.5β, 3β]	$Q_f Q_u f_{y0} t_0^2 \psi_2$ DPRT: $\psi_2 = 0.19\eta_2/\beta + 0.5$ CPRT: $\psi_2 = 0.4\eta_2/\beta + 1.5$
Chang [21]	DPRT	[0.4, 0.8]	[1, 2]	[1.5, 2]	$\geq 1-4t_0/b_0$	$Q_f[Q_u(f_{y0}t_0^2 + f_{y2}t_2^2) - f_{y2}t_2^2(1-\eta_2)(3-\beta)/(1-\beta)^{3/2}]$
EC3[23]	DPRT	$\leq$0.85①	$\geq 2t_1/t_0$	$\geq\eta+\sqrt{\eta_2(\eta_2-\beta)}$	$\geq 1-2t_0/b_0$	$k_n Q_u f_{y0} t_2^2$
CIDECT[24]	DPRT	$\leq$0.85①	$\geq 4t_1/t_0$-1	$\geq$2	[β/0.85, 1] $\geq$flat width	$Q_f Q_u f_{y0} t_2^2$
CECS[25]	DPRT	$\geq$0.25	$\geq 4t_1/t_0$-1	$\geq$2	[β/0.8, 1] $\geq$flat width	-
Lima[26]	DPRT	[0.25, 0.85]	$\leq$1	$\geq\eta+\sqrt{\eta_2(\eta_2-\beta)}$	$\geq 1-2t_0/b_0$	$k_n Q_u f_{y0}(t_0+t_2)^{1.9}$

Note: DPRT: doubler-plate reinforced T-joint, CPRT: collar-plate reinforced T-joint, Q_f : chord stress function coefficient by CIDECT[24], k_n : chord stress function coefficient by EC3[23], $Q_u = 2\left(\eta + 2\sqrt{1-\beta}\right)/(1-\beta)$, ① EC3[23] and CIDECT[24] takes b_1/b_2 $\leq$0.85 instead of b_1/b_0.

2. Finite element model and validation

2.1 General descriptions of the tests

The finite element (FE) package ABAQUS is adopted to investigate the static behavior of CPR SHS T-joints. In order to ascertain the accuracy and objectivity of the FE simulation scheme, 7 test specimens in relevant literature are cited for validation. These specimens including 3 UR T-joints with β ranged from 0.5 to 0.8, and 4 CPR T-joints with β ranged from 0.5 to 0.625 respectively[19,20,30]. The geometrical and material properties of the specimens are listed in Table 2, and the test setups are demonstrated in

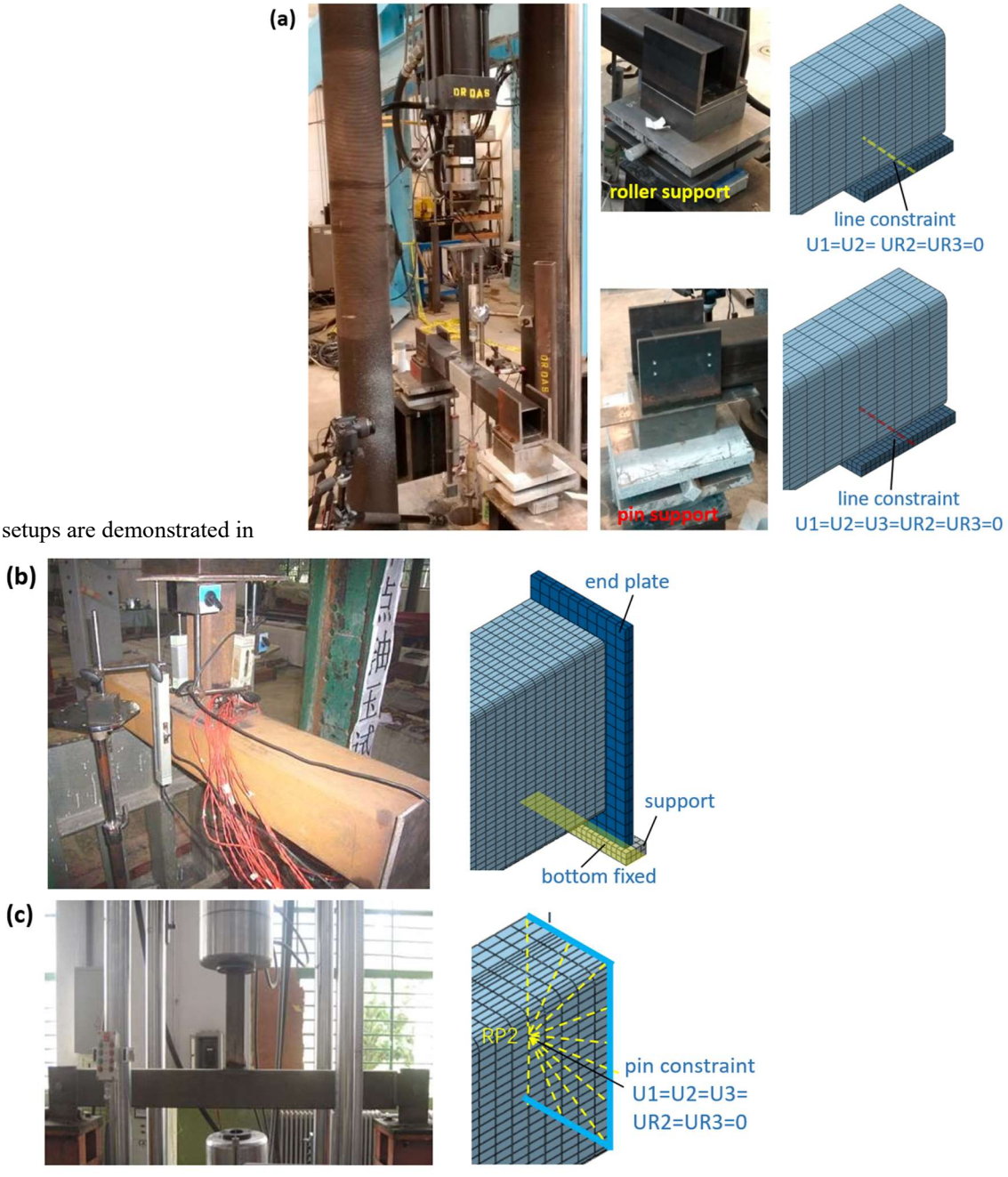

Fig. 3. The chord of joints tested by Ozyurt et al. [19] was supported by a roller at one end and a pin at the other end. For the tests by Feng et al. [20], the two ends of the chord were supported by endplates, which can be treated as simple supporting boundary. The joints by Wang et al. [30] were pinned at both ends of the chord. Considering the variety of dimensions and boundary conditions, these specimens are representative for the validation of the current FE model.

Table 2 Geometries[mm] and material properties[N/mm^2] of the specimens

Reference	Note	Type	β	Chord		Brace		Collar plate	
				b_0-h_0-t_0-L_0	f_{y0}- f_{u0}	b_1-h_1-t_1-L_1	f_{y1}- f_{u1}	b_2-h_2-t_2	f_{y2}- f_{u2}
Ozyurt[19]	U1	URT	0.5	102-102-4.8-	281.5-	51-51-4.8-500	399-438	-	
	C1-6	CPRT	0.5	1001	420.5	51-51-4.8-500	399-438	101-151-6	578-587
Feng[20]	TSCB80P6	CPRT	0.53	150-150-6-	327-	80-80-5-500	402-489	140-180-8	325-423
	TSCB80P8	CPRT	0.53	1000	418	80-80-5-500	402-489	140-180-6	310-411
	TSUB120	URT	0.8			120-120-5-500	334-426	-	
Wang[30]	3#	URT	0.625	160-160-4-	320-	100-100-4-400	320-412	-	
	4#	CPRT	0.625	2000	412	100-100-4-400	320-412	130-130-6	320-412

Note: b_i, h_i, t_i, L_i, f_{yi} and f_{ui} (i=0,1,2) are the width, the height, the thickness, the length, the yield strength and the ultimate strength of the members. The index 0, 1and 2 represent the chord, the brace and the CP respectively.

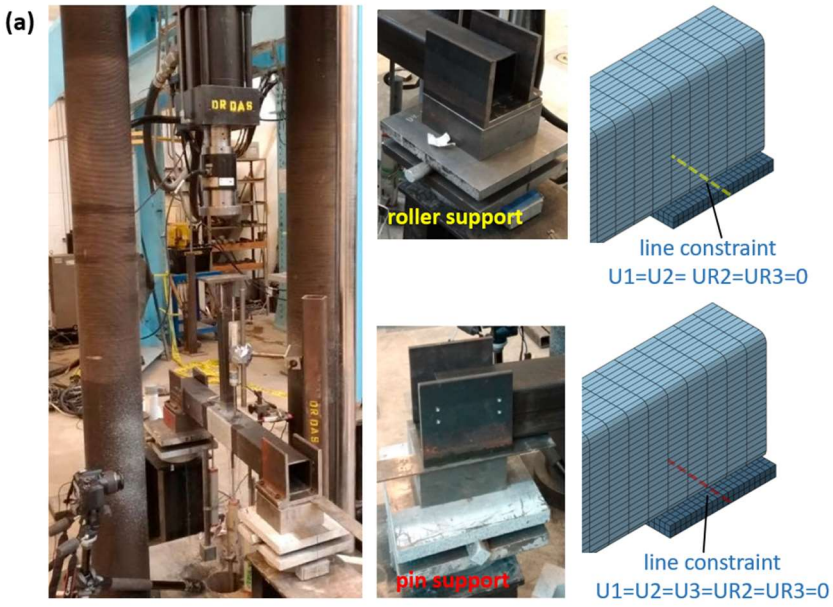

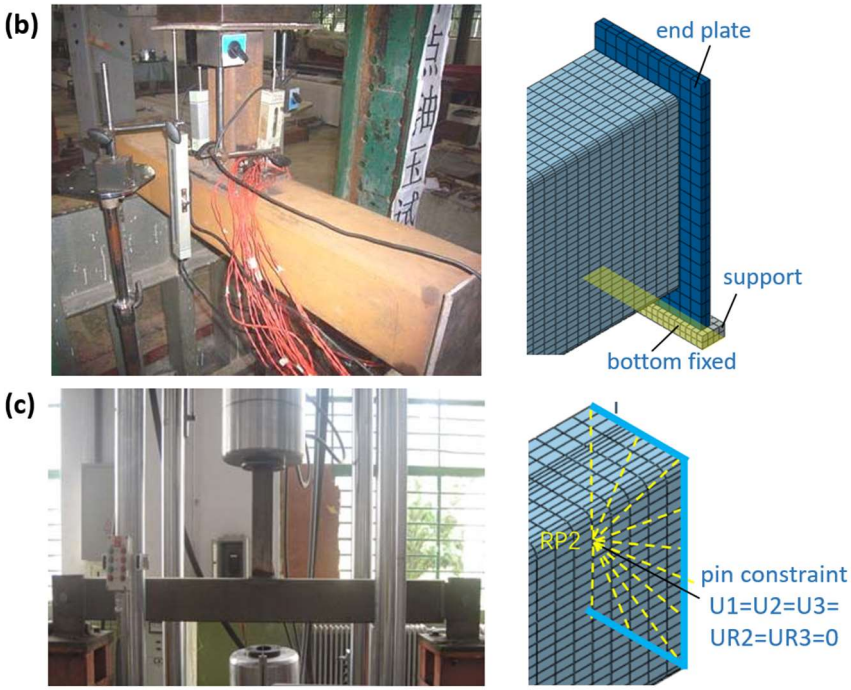

Fig. 3. Typical test setups of CPR SHS T-joints: (a) Ozyurt et al. [19]; (b). Feng et al. [20]; (c). Wang et al. [30].

2.2 Element type and meshing

Three-dimensional eight-node solid element with linear reduction integral element C3D8R is used to model the joint members and the connection welds. The interface between chord top flange and the CP underside was modeled using "surface to surface" contact, in which a "no friction" contact is applied in the tangential direction[5,19] and the "hard contact" is defined along the normal direction. The details of FE meshing are shown in Fig. 4(a), the meshing near the intersection zone between the chord and brace is refined to obtain accurate prediction of the joint, in view of the complex stress distribution in this region[31,32]. To obtain the optimal mesh size with the balance between accuracy and time-saving, convergence studies are also conducted. It can be found that assigning two elements in the thickness direction of the joint members, and setting 5mm mesh size in refined zones can achieve the optimized outcomes. The fillet welds between the brace, the chord flange, and the collar plate are modeled respectively, as shown by Fig. 4(b) and (c). The throat thickness of the welds are set as $1.1t_0$ [24], and the material property of the weld is the same as the chord.

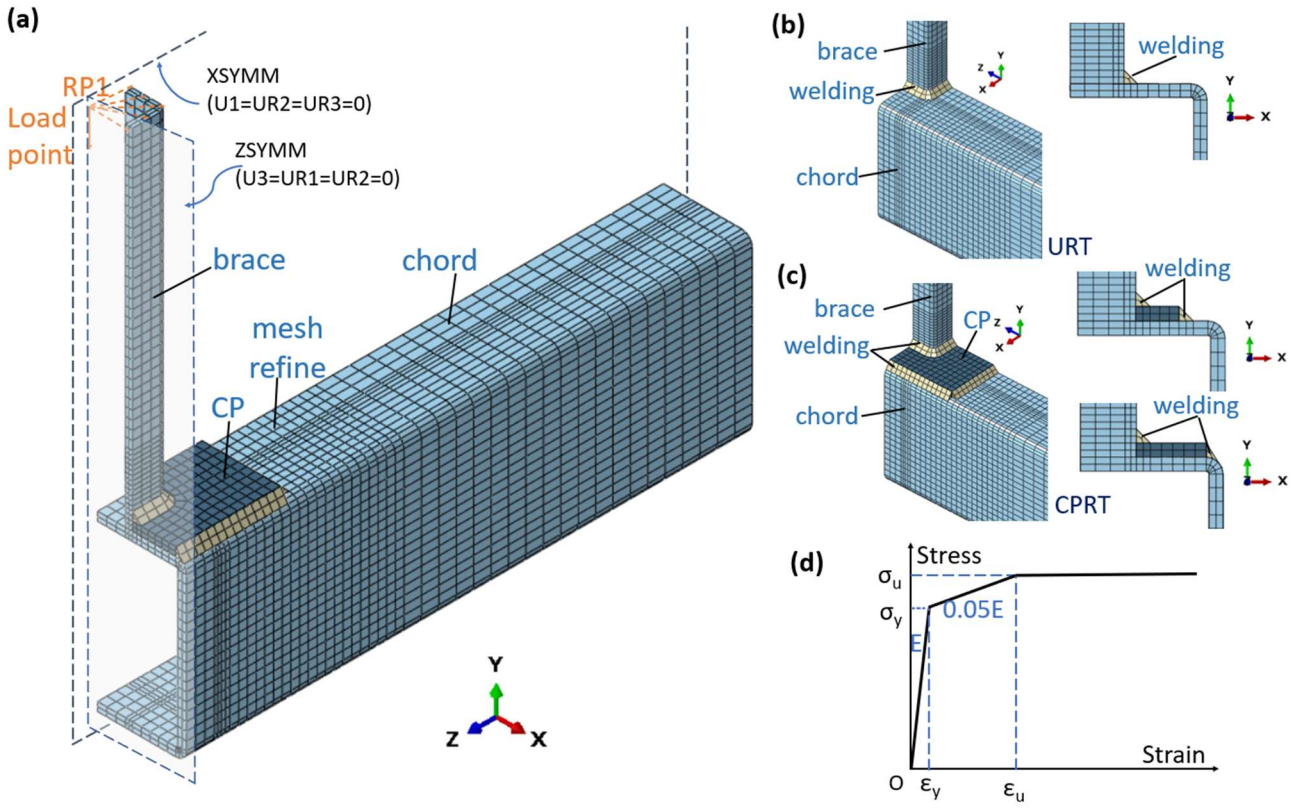

Fig. 4. Meshing details and material model of CPR SHS T-joints. (a) one quarter model, (b) unreinforced SHS joint, (c) CPR SHS joint, (d) material model

2.3 Nonlinearity of material model

The material nonlinearity is considered in modelling the joint members by a tri-linear elastic-plastic relationship stress-strain curve, as shown in Fig. 4 (d). The elastic modulus is assumed as E and the hardening modulus is assumed as 5/100th of the elastic modulus[2]. In Fig. 4(d), parameter σ_y and σ_u are the yield strength and ultimate strength, ε_y and ε_u are the corresponding yield strain and ultimate strain value. The input stress-strain curve in Fig. 4(d) is the true stress-strain model[2,19], which can be calculated from the engineering stress and strain from by Eq.(1) and Eq.(2):

$$\sigma_{true} = \sigma_{eng}(1 + \varepsilon_{eng}) \tag{1}$$

$$\varepsilon_{true} = ln(1 + \varepsilon_{eng}) \tag{2}$$

Where the notations of σ_{true} and ε_{true} are the true stress and true strain, σ_{eng} and ε_{eng} represents the engineering stress and engineering strain measured by the coupon tests[20,30].

2.4 Boundary conditions and load applying

The boundary conditions of the FE analysis are determined as the same as to the test setups, as shown in

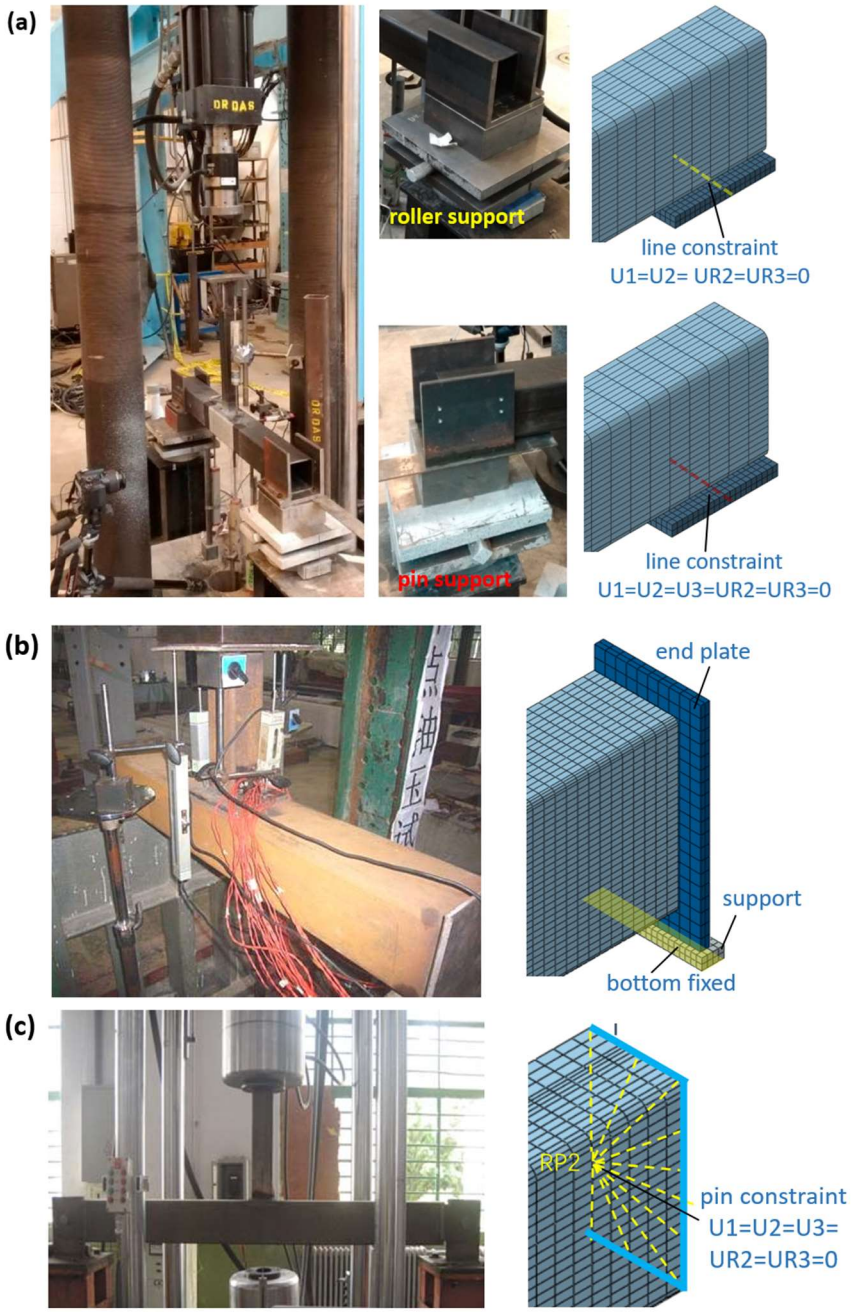

Fig. 3. For joints with same restraints on the chord ends [20,30], one quarter of the specimens are modelled and a symmetry constraint XSYMM and ZSYMM is applied. For joints with different restraints on the chord ends[19], half of the specimens are modelled and the symmetry constraint XSYMM is applied. A displacement control method is used to apply axial load on the brace, and the brace top end is coupled to a reference node RP1 by "coupling" constraint for the convenience of load applying. Node RP1 is allowed to move along the Y direction only, thus axial loads can be applied by controlling the vertical displacement of node RP1.

2.5 Validation

The reliability of the numerical model is evaluated from two aspects, namely the failure modes and the load-displacement curves, as shown in Fig. 5. It can be seen that the FE curves and failure modes agree well with the test results. It should be noted that the X-axis in Fig. 5 (a) represents the deformation difference between top and bottom flange of the chord, while the X-axis in Fig. 5 (b) denotes the displacement of the brace end. The comparison of the compressive strengths of the

specimens is summarized in Table 3, which further confirms the reliability of the FE models. The mean ratio between the FE results and the test data is 1.02, with a coefficient of variation (COV) of 0.027. Therefore, the current FE model is reliable for further parametric studies.

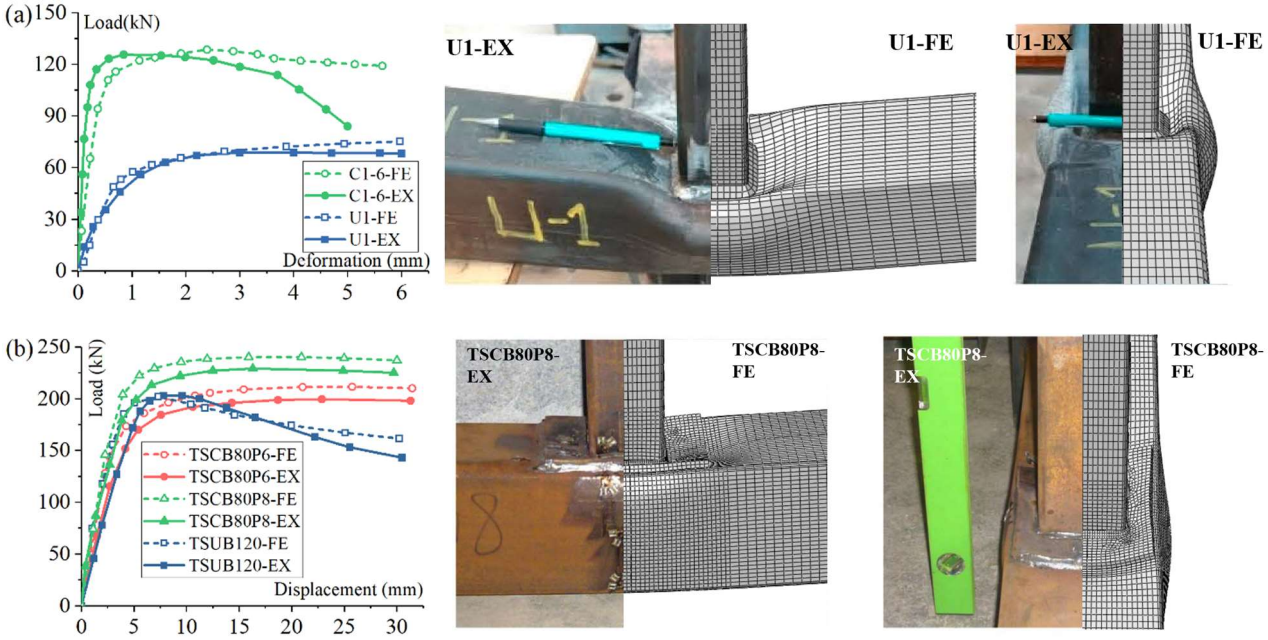

Fig. 5. Comparisons of the numerical results with the experimental tests. (a) Ozyurt et al.[19]; (b). Feng et al.[20].

Table 3 Compressive strength of the specimens by tests and FE analysis

Specimens	N_{ult}(kN)		$N_{ult\text{-}FE}$ / $N_{ult\text{-}EX}$
	EX	FE	
U1[19]	68.5	70.2	1.02
C1-6 [19]	125.8	128.5	1.02
TSCB80P6[20]	198.9	211	1.06
TSCB80P8 [20]	228.6	240.3	1.05
TSUB120[20]	205.1	201.2	0.98
3#[30]	49.5	51.2	1.03
4#[30]	87.2	86.1	0.99
Mean			1.02
COV			0.027

3 Parametric analysis

3.1 Parametric study strategy

After confirming the good agreement between the numerical and experimental results, the aforementioned FE models are adopted for further parametric studies. The geometries of the collar plate and the brace were mainly concerned, and the section of the SHS chord was determined as $b_0 \times h_0 \times t_0$=100×100×5 mm. The lengths of the chord and the brace were set as 650 mm and 300mm respectively. The perfect elastic-plastic material models were adopted for the chord, the weld and the CP to eliminate the influence of material hardening, previous studies indicated such assumption is adequate to predict the compressive behavior of the joints[2]. Several key points were needed to define the material model, namely the yielding strength is 345 N/mm^2, the elastic modulus is 2.0×10^5 N/mm^2, and the Possion ratio is 0.3. Furthermore, the chord

is continuously supported at the corner of the chord bottom to exclude the influence of overall bending of the chord[2,13]. For joints with no chord stress, the RP2 at the chord end is fixed, only the brace is axially loaded in compression by a single step, which defining the displacement of RP1. As for joints with chord stress, the non-proportional loading procedure is adopted, by which the chord stress is applied prior to the application of the brace axial load. In the first load step, the reference node RP2 is released to move freely along the longitudinal direction of the chord, by which the axial load can be applied on the chord (

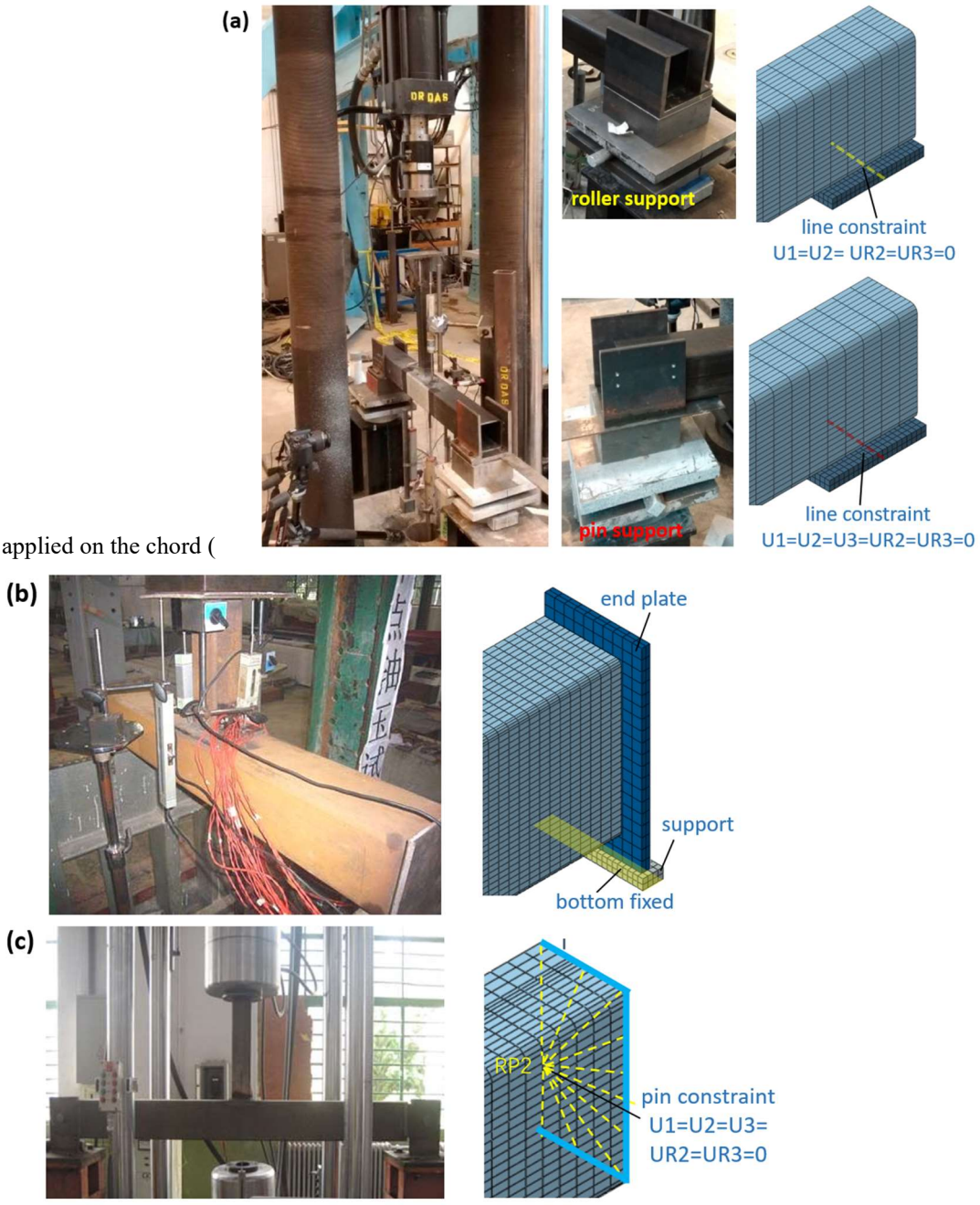

Fig. 3c). In the second load step, the chord stress is kept constant and the axial load is applied on the brace by RP1.

Five groups of parametric studies were designed and listed in Table 4. Firstly, a group of unreinforced and CP reinforced T-joints with the width ratio of β range from 0.4 to 0.8 were modeled to investigate the influence of brace width on unreinforced and CPR SHS joints in G1-1 and G1-2. Then, a series of CPR T-joints were modeled to study the effect of geometric dimension of CP on compressive performance: G2 changing the brace width and CP thickness when η_2 and γ_2 were fixed; G3 changing the width and thickness of CP when β=0.4 and γ_2=1.2; G4 changing the brace width, CP thickness

and CP length when η_2 was fixed. Finally, the chord stress ratio n ranged from -0.8 to 0.8 was applied to URT and CPRT joints with different β ratio when the geometric dimension of CP was fixed. In all, 29 URT and 96 CPRT joints were studied in this part. The chord stress ratio n can be calculated by Eq. (3) as following[23]:

$$n = \frac{N_0}{A \cdot f_{y0}} \tag{3}$$

where N_0 denotes the chord end load, A denotes the chord section area.

Table 4 Parametric matrix for CPR SHS T-joints

Note	β	τ_2	η_2	γ_2	n	Description
G1-1	0.4, 0.5, 0.6,	-	-	-	0	Change β of URT
G1-2	0.7, 0.8	1	0.9	1.2	0	Change β of CPRT
G2	0.4, 0.6, 0.8	1.0, 1.4, 1.8, 2.2, 2.6	0.9	1.2	0	Change β & τ_2 of CPRT
G3	0.4	1.0, 1.4, 1.8, 2.2, 2.6	0.5, 0.7, 0.9	1.2	0	Change τ_2 & η_2 of CPRT
G4	0.4, 0.6, 0.8	1.0, 1.4, 1.8, 2.2, 2.6	0.9	0.9, 1.2, 1.5, 1.8	0	Change β, τ_2 & γ_2 of CPRT
G5-1	0.4, 0.6, 0.8	-	-	-	0, ±0.2, ±0.4,	Change n for URT
G5-2	0.4, 0.6, 0.8	1	0.9	1.2	±0.6, ±0.8	Change n for CPRT

To eliminate the effects of chord material properties and dimension, the normalized load-deformation curves are commonly used [2,4,21], by which two dimensionless parameters are employed, as shown by Eq. (4) and Eq. (5).

$$\overline{N_0} = \frac{N}{f_{y0} \cdot t_0^2} \tag{4}$$

$$\overline{\delta_0} = \frac{\delta}{b_0} \tag{5}$$

where $\overline{N_0}$ and $\overline{\delta_0}$ are the normalized load and displacement on the brace, N and δ are the actual axial load and displacement on the brace of the joints, f_{y0} is the yielding strength of the chord, t_0 and b_0 are the thickness and width of the chord. By using the $\overline{N_0} - \overline{\delta_0}$ curves, the normalized ultimate strength of the joint can be determined by 3% displacement criterion of Zhao et.al [33], and was denoted as $\overline{N_u}$. To further evaluate the reinforcement efficiency of the collar plate, another parameter S_e is introduced and expressed as shown by Eq. (6).

$$S_e = \frac{\overline{N_u^R}}{\overline{N_u^{UR}}} \tag{6}$$

Where $\overline{N_u^R}$ represents the normalized ultimate strength of the CPR T-joint, and $\overline{N_u^{UR}}$ represents the normalized ultimate strength of the corresponding unreinforced joint.

3.2. Influence of the Width of the Brace (G1)

The axial compressive behavior of SHS T-joints was investigated in group G1 by changing the value of β from 0.4 to 0.8. Fig. 6(a-b) demonstrate the normalized load-displacement curves of URT (G1-1) and CPRT (G1-2) joints. It is shown that both the ultimate load and the initial stiffness of URT and CPRT joints are significantly improved as β increased. For the URT joints with $\beta \leq 0.8$, the $\overline{N_0} - \overline{\delta_0}$ curves are smooth and no peak load is found, which demonstrates the yield of the chord surface occurred and dominated [2]. The trend for CPRT curves with $\beta \leq 0.6$ is similar to that of URT ones, however, a peak load is found for CPRT curves with $\beta \geq 0.7$, which indicates that the failure mode of chord web buckling dominated [21]. This can be proved by Fig. 6 (c), in which the out of plane displacement (U1 contours at $\delta = 3\% b_0$) of CPRT joint increases obviously as β increased for 0.6 to 0.8. The change of the failure mode mainly due to the “over-reinforcement”

of the collar plate on the chord flange, which has also been observed by the doubler plate reinforced SHS T-joint with large β value [22]. In the view of full utilization of the reinforcement plate, the collar plate is more suitable of SHS joints with $\beta \leq 0.7$. For joints with $\beta > 0.7$, the side plate reinforcement [13,23] as well as the L-shape collar plate[14] can be adopted to reinforce the side wall of the chord.

The "over-reinforcement" effect also influences the strength and reinforcement efficiency of the CPRT joints, as shown in Fig. 6 (d). When β increases from 0.4 to 0.8, the normalized ultimate strength of CPRT joint increased 136%, which is much lower than 259% for URT joint. This also leads to the decrease of reinforcement efficiency, it can be seen from Fig. 6 (d) that the S_e factor decreases from 2.16 to 1.41 when β increases from 0.4 to 0.8. Nevertheless, the collar plate is effective to reinforce the SHS joint. For example, the strength of CPRT joint with β=0.4 is even 24% higher than that of URT joint with β=0.6. The reinforcement effect of the collar plate is shown by Fig. 6 (e), in which the U2 contours for URT and CPRT joints with different β ratio at δ=3%b_0 are compared. It can be seen from Fig. 6(e) that the collar plate deforms coordinately with the chord flange and enlarges the yielding range of the chord surface as β increased, which is similar to the findings of doubler plate reinforcement [19,20].

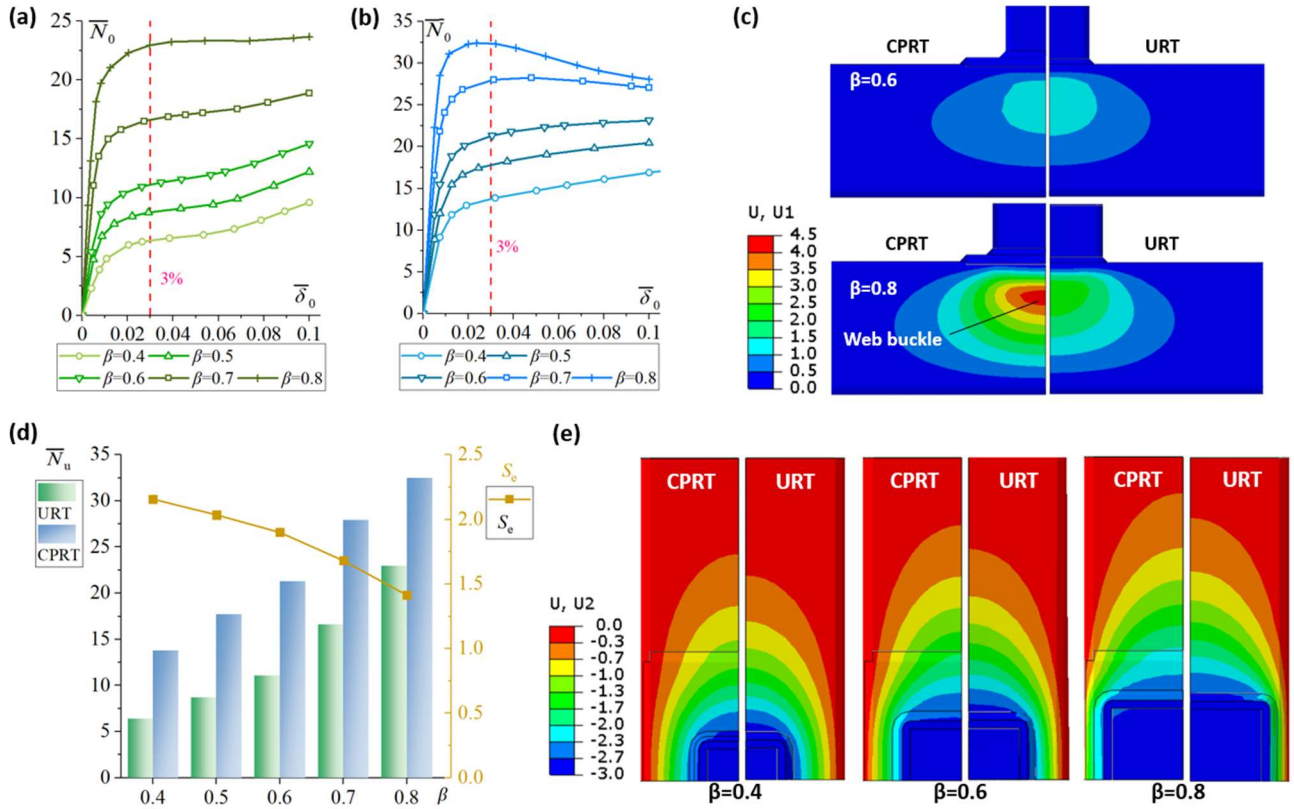

Fig. 6. Influence of β (G1): (a). $\overline{N_0} - \overline{\delta_0}$ curves of URT; (b). $\overline{N_0} - \overline{\delta_0}$ curves of CPRT; (c). U1 Contours under 3%b_0 brace end displacement. (d). Change of $\overline{N_u}$ and S_e with β; (e). U2 Contours under 3%b_0 brace end displacement.

3.3 Influence of the thickness of CP (G2)

In group G2, the thickness of the collar plate was changed for CPRT joints with the β ratio of 0.4, 0.6 and 0.8. The value of τ_2 varied in a wide range from 1.0 to 2.6, while η_2 and γ_2 was kept unchanged. The $\overline{N_0} - \overline{\delta_0}$ curves of G2 are compared in Fig. 7(a-c), by which the strength of the joint increased with the increase of τ_2. However, the enhance effect of τ_2 decreased as β ratio increased, for example the curves in Fig. 7 (c) are close to each other. By comparing the $\overline{N_u}$ in Fig. 7 (d), it can be seen the normalized ultimate strength of CPRT joint with β=0.4 increased 132% as τ_2 increased from 1.0 to 2.6, which is far larger than 15% of joint with β=0.8. The reason is also the "over-reinforcement" effect of thick collar plate

on the chord flange, which leads to buckling of the chord web.

The reinforcement efficiency of CPRT joints with various β and τ_2 is shown in Fig. 7(e). It can be seen that the value of S_e increased with the increase of τ_2. When τ_2 increased from 1.0 to 2.6, S_e increased from 2.16 to 5.02 for CPRT joint with β=0.4. The trend of reinforcement efficiency with the change of β ratio is similar to G1, and a thicker collar plate may lead to more descending of S_e as β ratio increased. For example, the decrease of S_e factor is 67% for CPRT joint with τ_2=2.6 when β increases from 0.4 to 0.8, which is larger than 34% for CPRT joint with τ_2=1.0. Therefore, a thick collar plate is not necessary for SHS joints under compression. The thickness of τ_2=1.0 is recommended for the SHS joints with $\beta \geq 0.7$, and τ_2 =[1.0, 2.0] is recommended for joints with β<0.7.

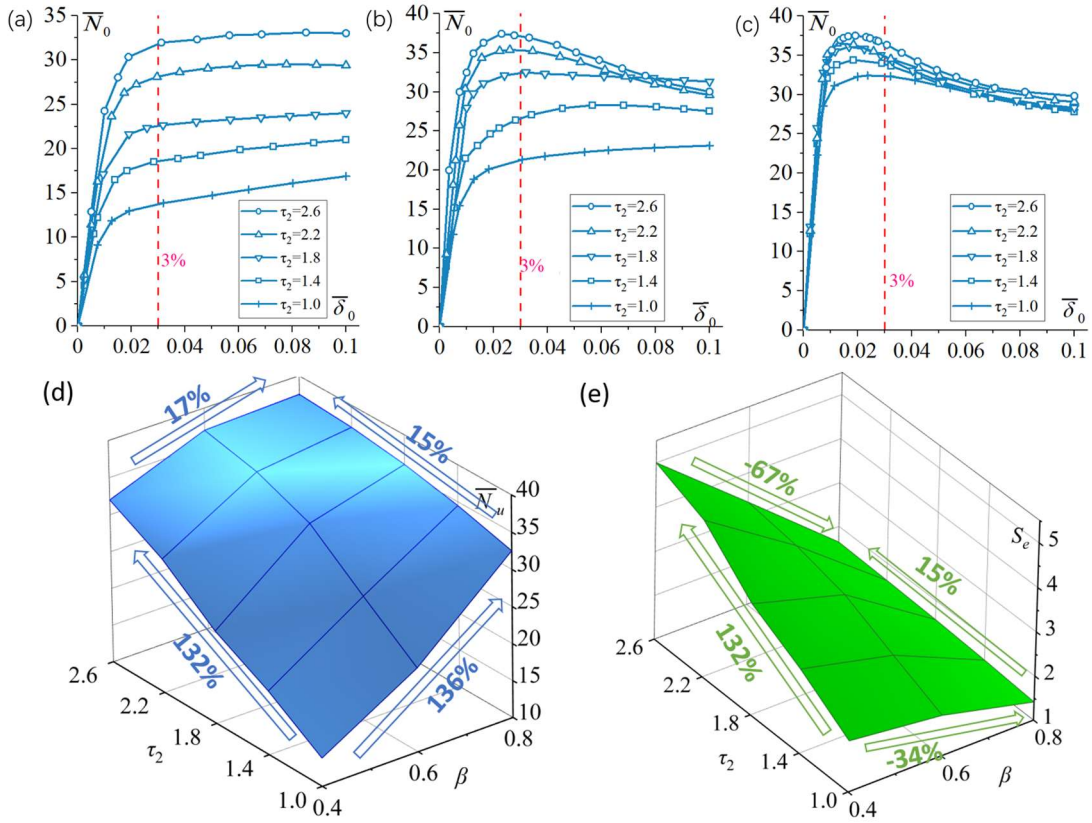

Fig. 7. Influence of τ_2 (G2): (a). $\overline{N_0} - \overline{\delta_0}$ curves of CPRT with β=0.4; (b). $\overline{N_0} - \overline{\delta_0}$ curves of CPRT with β=0.6; (c). $\overline{N_0} - \overline{\delta_0}$ curves of CPRT with β=0.8; (d). Normalized ultimate strength of CPRT; (e). Reinforcement efficiency of CPRT.

3.4 Influence of the width of CP (G3)

Although the collar plate has been recommended to be equal width with the flat surface of the chord by several literatures [19,23,24], the experimental tests indicated that the equal width collar plate have to weld on the corner of the chord, which will cause welding difficulties as well as potential brittle crack risk of the welding[4]. Therefore, the influence of the width of the collar plate was investigated in group G3, to further check the suitability of narrow collar plate. Considering there is not enough gap to change the width of collar plate for joints with high β ratio, only the CPRT joints with β=0.4 are concerned. The length of the collar plate was fixed as $1.2b_0$, and the width of the collar plate was varied from $0.5b_0$ to $0.9b_0$. Moreover, the thickness of the collar plate was varied by changing τ_2 from 1.0 to 2.6. The typical $\overline{N_0} - \overline{\delta_0}$ curves of G3 are plotted in Fig. 8 (a), it can be seen both the strength and initial stiffness are improved apparently by increasing the width of the collar plate.

It can be seen in Fig. 8 (c) that the thicker of the collar plate, the more effective of η_2. For example, the increase of $\overline{N_u}$ is up to 176% as η_2 increased from 0.5 to 0.9 for joints with τ_2=2.6, comparing to 47% of the joint with τ_2=1.0. The influence of collar plate width on S_e is quite similar to that of $\overline{N_u}$ as shown by Fig. 8 (d). The highest reinforcement efficiency is up to 5.02 for CPRT joint with η_2=0.9 and τ_2=2.6. This mainly due to the width of the collar plate will influence the development of yielding on it, as shown by the U2 contours in Fig. 8 (b). For narrow collar plate with η_2=0.5, little yielding behavior is observed and the collar plate is not fully utilized. While for joints with η_2=0.9, the collar plate bend along the width direction and more yielding is developed, which results in more enhancement on the joint. Therefore, a wider collar plate is more effective to enhance the compressive strength of the SHS joint, and the recommendations by EC3[23] and CIDECT[24] are reasonable. For easy welding consideration as well as to reduce the risk of brittle cracking, the L-shape collar plate is one optional method[14]. Another option is to modify the suggestions of EC3[23] by $\eta_2 = (b_f - t_w)/b_0$, where b_f and t_w refers to the flat width of the chord flange and the throat thickness of the weld.

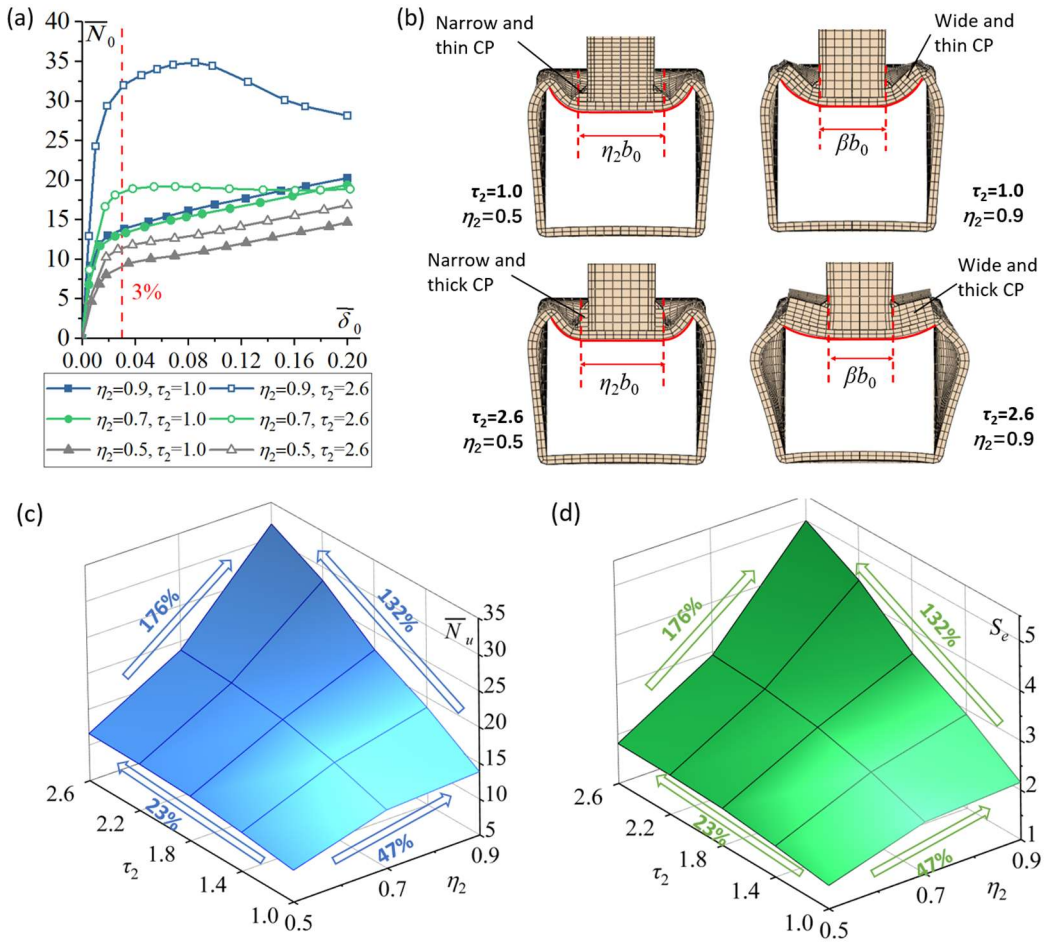

Fig. 8. Influence of η_2 (G3): (a). Typical $\overline{N_0} - \overline{\delta_0}$ curves of CPRT with β=0.4; (b). Deformation under 20%b_0 brace end displacement level; (c). Normalized ultimate strength of CPRT; (d). Reinforcement efficiency of CPRT.

3.5 Influence of the length of CP (G4)

In group G4, the effect of the length of the collar plate was investigated. To check the interacting between the collar plate length and thickness as well as the width ratio, the parameters β and τ_2 were also changed. By comparing the trends of $\overline{N_u}$ and S_e in Fig. 9 (a) and (b), it can be seen that the length of the collar plate has little influence on the compressive behavior of CPRT joints, the increases of $\overline{N_u}$ for joints with β =0.4, 0.6 and 0.8 are 12.4%, 12.7% and 14.6% by increasing γ_2 from 0.9 to 1.8. This is mainly due to the fact that there is a certain range of yielding length on the chord surface and the collar

plate as shown in Fig. 9 (c), the yielding length will not increase when γ_2 exceeds 1.5. Moreover, the change of τ_2 also leads to little influence on the $\overline{N_u}$-γ_2 trend, as shown in Fig. 9 (d) to (f). The minimum γ_2 values by EC3[23] and CIDECT[24] were also marked out by dash lines in Fig. 9 (d) to (f), and the recommendation of EC3[23] seems more reasonable than CIDECT[24]. Considering the length of the collar plate is not as influential as the width and the thickness, the range of γ_2 is recommended between the range of 1.0 and 1.4.

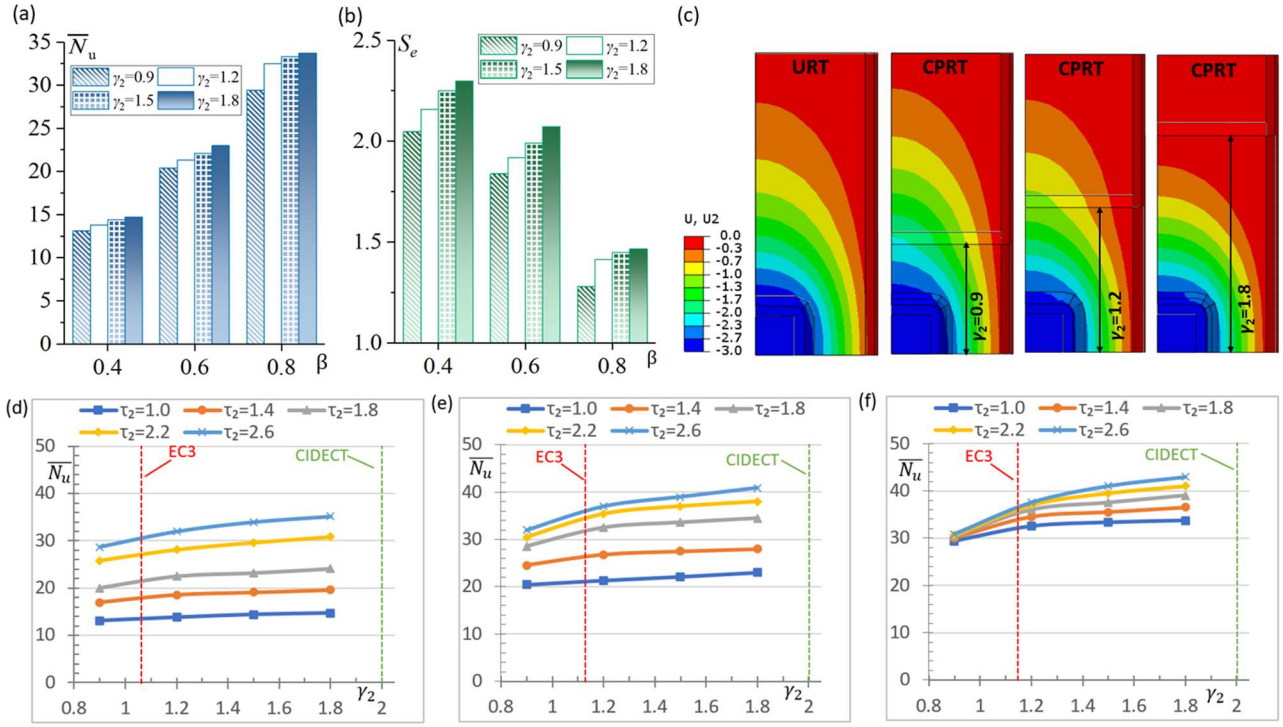

Fig. 9. Influence of β&γ_2 (G4): (a). Normalized ultimate strength of CPRT; (b). Strengthen efficiency of CPRT; (c). Contours of U2 under 3%b_0 brace end displacement level; (d) $\overline{N_u}$-γ_2 trend of CPRT with β=0.4; (e) $\overline{N_u}$-γ_2 trend of CPRT with β=0.6; (f) $\overline{N_u}$-γ_2 trend of CPRT with β=0.8.

3.6 Influence of chord axial stress ratio (G5)

To investigate the influence of axial stress ratio on the chord, the value of n was changed from -0.8 to 0.8 and the $\overline{N_0} - \overline{\delta_0}$ curves are compared in Fig. 10. Meantime, a series of typical contours of Von Mises stress are captured in Fig. 11 to illustrate the impact of chord axial stress ratio on joint yielding range. It can be seen from the curves of Fig. 10 (a) to (c) for URT joints that the tensile stress on the chord is less influential than that of the compressive stress, which agrees well with the existing studies on unreinforced joints [34]. The influence of chord tensile stress on CPRT joints is quite similar to that on URT joints, as shown by Fig. 10 (d) to (f). However, the influence of chord compressive stress on CPRT joints is different with that on URT joints, the presence of the collar plate seems to relief the negative effect of the chord compressive stress ratio. The normalized strengths of the joints are further compared in Fig. 12, by which less reduction of the strength is found for CPRT joints than the URT ones. For example, the reduction ratio of $\overline{N_u}$ for CPRT joints with β =0.4 and 0.6 are 6.2% and 5.7% by increasing n from 0 to -0.8, which are lower than 18.8% and 16.4% for URT joints.

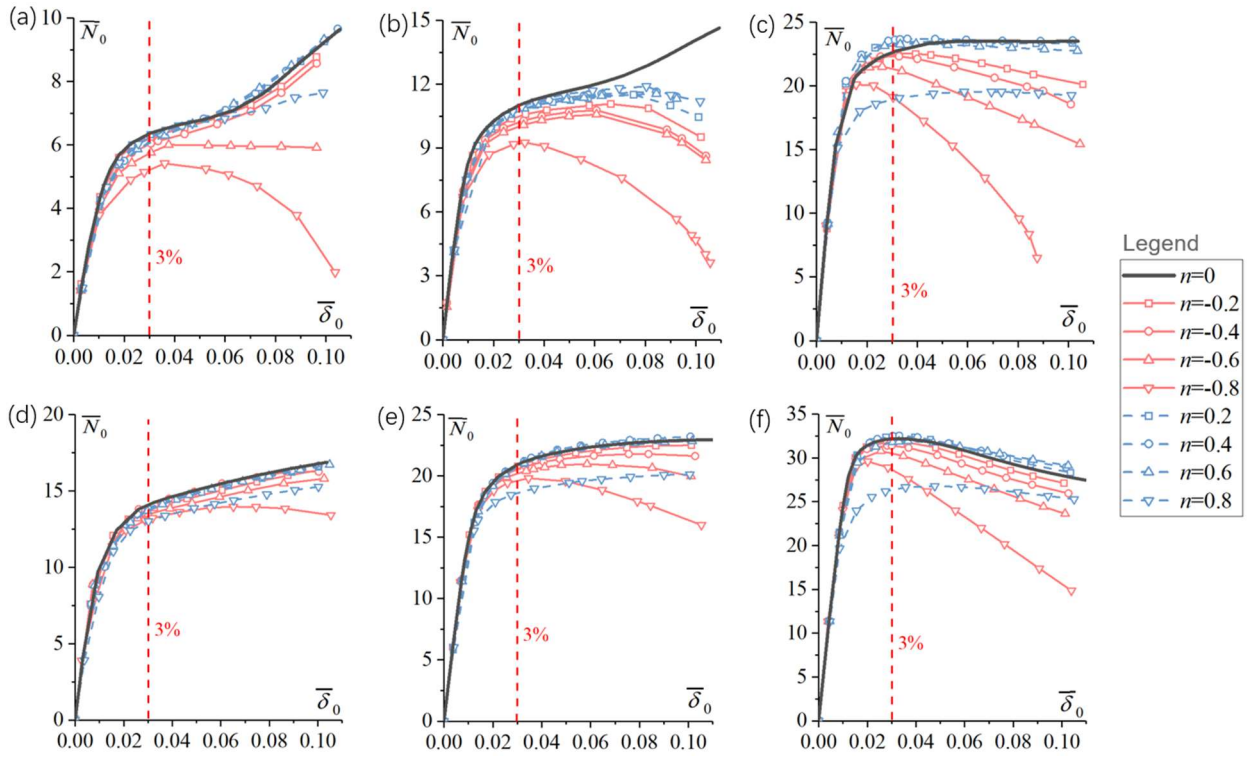

Fig. 10. Influence of n (G5) on $\overline{N_0} - \overline{\delta_0}$ curves: (a). URT with β=0.4; (b). URT with β=0.6; (c). URT with β=0.8; (d). CPRT with β=0.4; (e). CPRT with β=0.6; (f). CPRT with β=0.8.

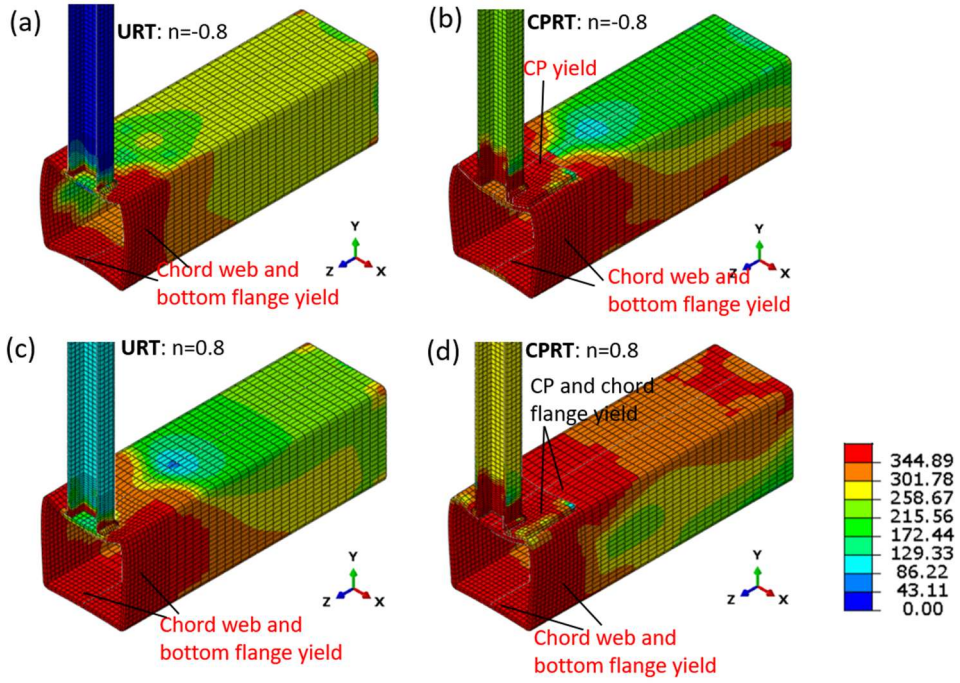

Fig. 11. Contours of Von Mises stress under 3%b_0 brace displacement level with different n (G5): (a). URT with n=-0.8; (b). CPRT with n=-0.8; (c). URT with n=0.8; (d). CPRT with n=0.8.

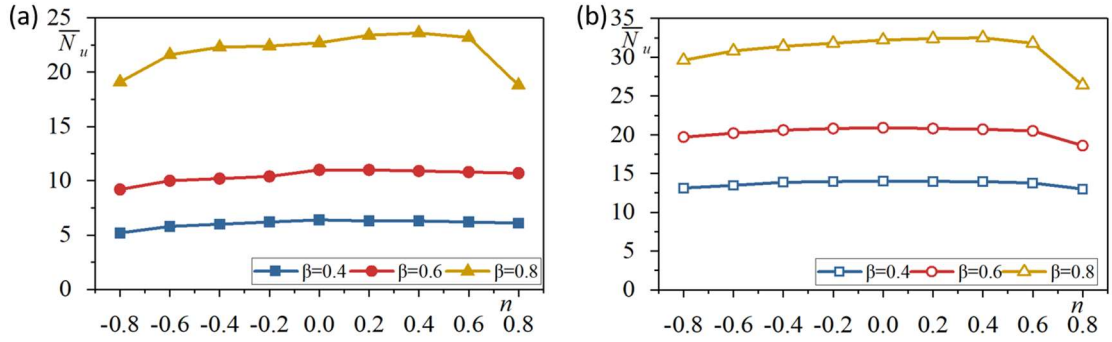

Fig. 12. Influence of n (G5) on normalized strength of joints: (a). URT; (b). CPRT.

4 Discussions

4.1 Key parameters and suggestions for collar-plate size

The influence of each parameter has been investigated in section 3, and the values of geometrical parameters β, η_2, γ_2 and τ_2 are shown to be influential. To identify the key parameters, the CPRT joint with β=0.4, η_2=0.9, τ_2=1.0 and γ_2=0.9 is taken as the reference specimen, and then each parameter is doubled respectively to compare the growth rate of $\overline{N_u}$ in Fig. 13. It can be seen from Fig. 13 that by double the value of β, γ_2 and τ_2, the increase of $\overline{N_u}$ is 124%, 12% and 75% respectively. Since the value of η_2 was restrained by the width of the chord flange and cannot be doubled, the CPRT joint with β=0.4, η_2=0.5, τ_2=1.0 and γ_2=0.9 was taken for comparison, and the increase of $\overline{N_u}$ is 41% by increasing η_2 from 0.5 to 0.9.

On the basis of the parametric analysis, as well as to consider the reinforcing efficiency, the dimensions of the collar plate are suggested as follows:

(1) Width: equal to the flat width of the chord flange, or η_2=1-3/γ.

(2) Length: 1.0≤ γ_2 ≤1.2

(3) Thickness: 1.0 ≤ τ_2 ≤ 2.0 for joints with β<0.8, and τ_2 = 1.0 for joints with β ≥ 0.8.

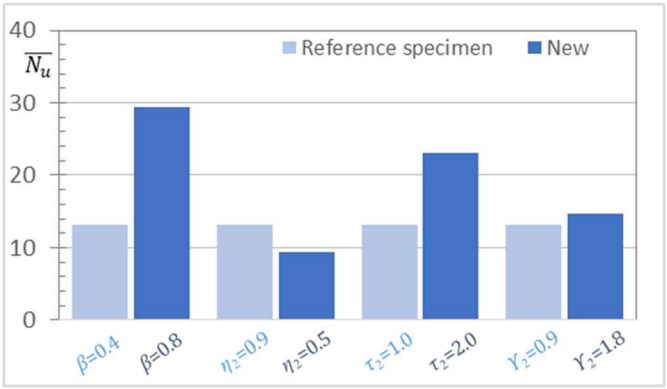

Fig. 13. Comparison of normalized strength by changing the parameters

4.2 Control failure modes

As demonstrated by the finite element analysis, the failure of CPRT joints under brace compression load is not only determined by β, but also by the width ratio of η_2 and the thickness ratio of τ_2. There are three failure modes were observed for CPRT joints, namely: chord flange yielding (M1), chord flange and collar plate yielding (M2), and chord web buckling (M3).

The failure of chord flange yielding (M1) is only found in group G3 for CPRT joints with β=0.4 and η_2≤0.7, where the

plastic hinge developed on the chord flange, as shown in Fig. 14 (a). This is mainly due to the width of the collar plate is small and little bending behavior occurred on it. In this situation, the collar plate plays the role to enlarge the compression area on the chord flange, and thus enhance the compressive strength of the joint.

As the value of η_2 increased to 0.9, failure mode M1 changed to the yielding of chord flange and collar plate (M2), as shown in Fig. 14 (b). The failure of M2 is found to dominate for all the joints with η_2=0.9 and β=0.4, as well as for joints with η_2=0.9, β=0.6 and $\tau_2 \leq 1.8$. It can be seen from Fig. 14 (b) that the contact between the collar plate and the chord flange is tight under compression, and several plastic hinges developed on the chord flange and the collar plate. Therefore, the role of the collar plate is to yield together with the chord flange, by which more enhancement of the strength is achieved than that of failure mode M1.

For joints with large β ratio or thick collar plate, the chord web buckling occurred, as shown in Fig. 14 (c). The FEA indicated that the failure mode M3 will dominate for all the CPRT joints with β=0.8, and for joints with β=0.6 and $\tau_2 \geq 2.2$. This is due to "over-reinforcement" on the chord flange by the collar plate, and the chord web buckling occurred in ahead of failure mode M2.

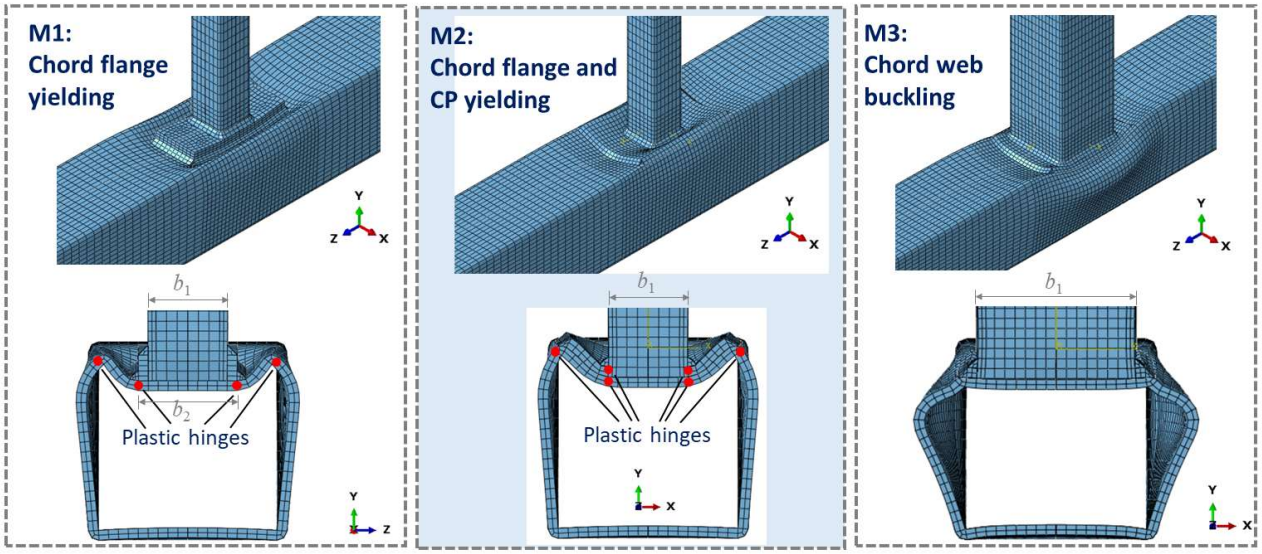

Fig. 14. Control failure modes for CPRT joints under brace compressive load

4.3 Chord stress function

The chord stress ratio will influence the development of yielding lines and thus need to be considered for unreinforced SHS joints. Currently, the k_n coefficient is introduced by EC3[23] and Q_f coefficient is introduced by CIDECT[24] to account for the influence of chord stress ratio, as quoted by Eq.(7) and (8).

$$k_{n,EC3}{}^{[23]} = \begin{cases} 1.3 - \frac{0.4|n|}{\beta} \leq 1.0, & n < 0 \\ 1.0, & n \geq 0 \end{cases} \tag{7}$$

$$Q_{f,CIDECT}{}^{[24]} = \begin{cases} (1-|n|)^{0.6-0.5\beta}, & n < 0 \\ (1-|n|)^{0.1}, & n \geq 0 \end{cases} \tag{8}$$

The k_n or Q_f coefficients for URT and CPRT joints from group G5 are plotted in Fig. 15, in which the curves predicted by EC3[23] and CIDECT[24] are also presented for comparison. It can be seen that the Q_f values for CPRT joints are quite

different from that for URT joints, especially when n<0. The curves by CIDECT[24] is safe for most of the URT joints, while the equation of EC3[23] provides unsafe predictions for joints with n>0 and joints with low compression stress ratio on chord. Moreover, the estimation by Eq. (8) for n>0 agrees well with the FEA data of URT and CPRT joints. However, it seems too conservative for CPRT joints with n<0, and modification can be done by Eq. (9) to achieve more reasonable predictions, as shown in Fig. 15.

$$Q_{f,NEW} = \begin{cases} (1-|n|)^{0.1-0.05\beta}, & n < 0 \\ (1-|n|)^{0.1}, & n \geq 0 \end{cases} \tag{9}$$

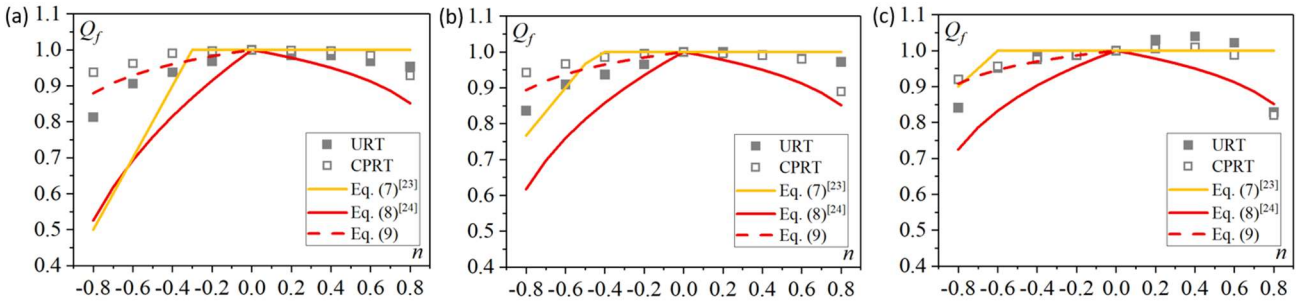

Fig. 15. Q_f coefficients for SHS T-joint: (a). β=0.4; (b). β=0.6; (c). β=0.8.

5. Compressive strength equations for CPR SHS T-joints

5.1. Design formulae based on failure modes

For unreinforced SHS T-joints under compression, two failure modes have been defined to dominate the strength of the joint, namely the chord flange yielding and the chord web buckling. The corresponding design formulae by EC3[23] and CIDECT[24] are quoted as follows:

$$\beta \leq 0.85 \quad N_{\text{URT-1}} = Q_f Q_u \cdot f_{y0} t_0^2 \tag{10}$$

$$\beta = 1.0 \quad N_{\text{URT-2}} = Q_f \cdot 2\chi f_{y0} t_0 (h_1 + 5t_0) \tag{11}$$

Where $N_{\text{URT-1}}$ and $N_{\text{URT-2}}$ denote the compressive strength of URT joint failure by chord flange yielding and the chord web buckling, a linear interpolation can be adopted for joints with 0.85< β < 1.0. $Q_u = 2\left(\eta + 2\sqrt{1-\beta}\right)/(1-\beta)$ gives the influence function for the parameters β and η. χ is the reduction factor for flexural buckling obtained from EN 1993-1-1 by using the relevant buckling curve. As mentioned in section 4.2, the control failure modes for CPRT joints under compressive load include three types: chord flange yielding (M1), chord flange and collar plate yielding (M2), and chord web buckling (M3). Therefore, these failure modes are concerned respectively to build design equations for the compressive strength of CPRT joints.

- Failure mode M1:

For failure mode M1, the collar plate is rigid enough to transfer the compressive load directly to the chord flange, by which the yield range on the chord flange is enlarged as shown in Fig. 16 (a). The parametric study indicates that the length of the collar plate is ineffective to increase the strength of failure mode M1, thus the effect range of the collar plate can be assumed to be square in Fig. 16 (a). By doing so, the parameters of β and η in Eq. (10) can be substituted by η_2, and the following equation is obtained:

$$N_{\text{CPRT-M1}} = Q_{f,NEW} \cdot \frac{2(\eta_2 + 2\sqrt{1-\eta_2})}{1-\eta_2} \cdot f_{y0} t_0^2 \tag{12}$$

- Failure mode M2:

For the failure of M2, the collar plate concaves together with the chord flange, and yielding lines develop on them both. Former studies on doubler plate reinforced SHS joint have proved that the presence of reinforcement plate did not change the yielding behavior of the chord flange[21], which is also adoptable for the CPRT joints. By comparing the typical concave contours of the chord flange and the collar plate in Fig. 16 (b), it can be seen quite similar deformation patterns are demonstrated on them. However, it should be noted that there exists a complicated interaction between the collar plate and the chord flange under compressive load. For example, the concavation of the chord flange changes the restraint condition of the collar plate, which will reduce the reinforcement effect. Therefore, a reduction factor of η_2/τ_2 is introduced to modify the yielding strength of the collar plate. By which the compressive strength of CPRT joints controlled by the co-yielding of the collar plate and the chord flange can be calculated by the following equation:

$$N_{\text{CPRT-M2}} = Q_{f,NEW} \cdot \frac{2(\eta+2\sqrt{1-\beta})}{1-\beta} \cdot (f_{y0}t_0^2 + f_{y2}t_2^2 \cdot \frac{\eta_2}{\tau_2}) \quad (13)$$

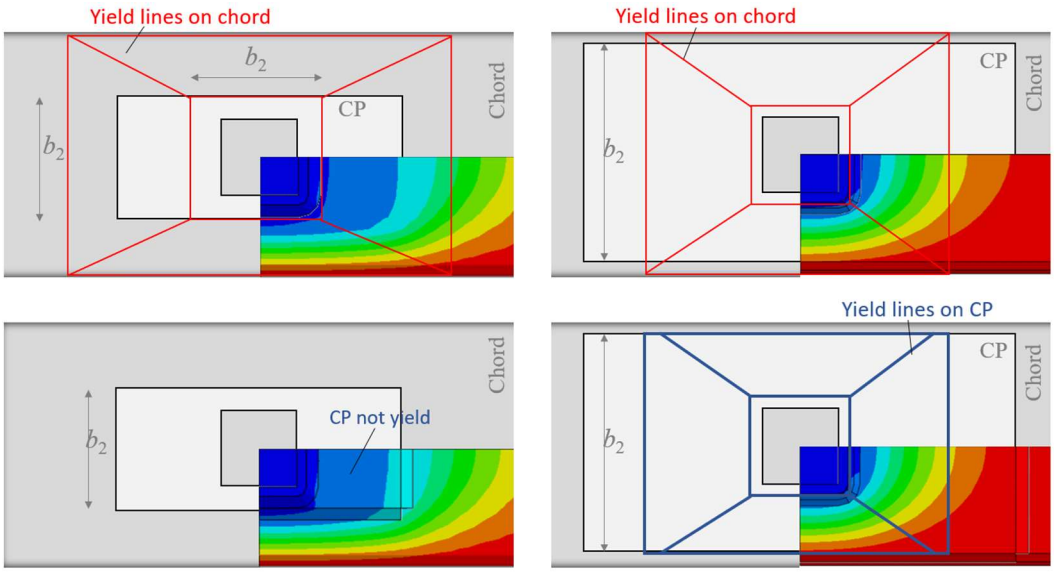

(a). M1 (b). M2

Fig. 16. Yielding lines of CPRT joints failed in M1 and M2.

- Failure mode M3:

Although the failure mode of M3 is controlled by the buckling of the chord web, the parametric study indicated that the buckling strength increased slightly as the length and thickness of the collar plate increased. This is probably due to the collar plate provides restraint for the chord web and elongates the buckling length on it. To account for this contribution, Eq. (11) was modified by introducing two parameters about the length and thickness of the collar plate.

$$N_{\text{CPRT-M3}} = Q_{f,NEW} \cdot 2\chi f_{y0}t_0[h_1 + 5t_0 + 0.2(L_2 - h_1) + 2.0t_2] \quad (14)$$

Where the values of 0.2 and 2.0 are determined by regression analysis on the data of the parametric study.

5.3. Assessment of the formulae

To assess the accuracy of the proposed formulae, the predicted normalized ultimate strengths of CPRT joints are compared with that obtained by the FEA, as shown in Fig. 17 (a). It can be seen from Fig. 17 (a) that the average ratio of design strength to FE results is 0.845 with R^2=0.934, which shows reasonable accuracy of the formulae. Meanwhile, the proposed formulae are safe for the design purpose, for example more than 90% of the ratio points are located between 60% to 100%.

Furthermore, the equation and FE results for CPRT joints with chord stress are also compared by Fig. 17 (b), in which the predictions by equations for DPR joints of EC3[23] and CIDECT[24] are also employed for comparison. It can be seen that the proposed Q_f coefficients in Eq.(9) is acceptable to account for the influence of chord stress ratio, by which the predicted strength is 87.6% to the FE ones with a R^2=0.990. The predictions by EC3[23] and CIDECT[24] are safe yet too conservative for CPR T-joints.

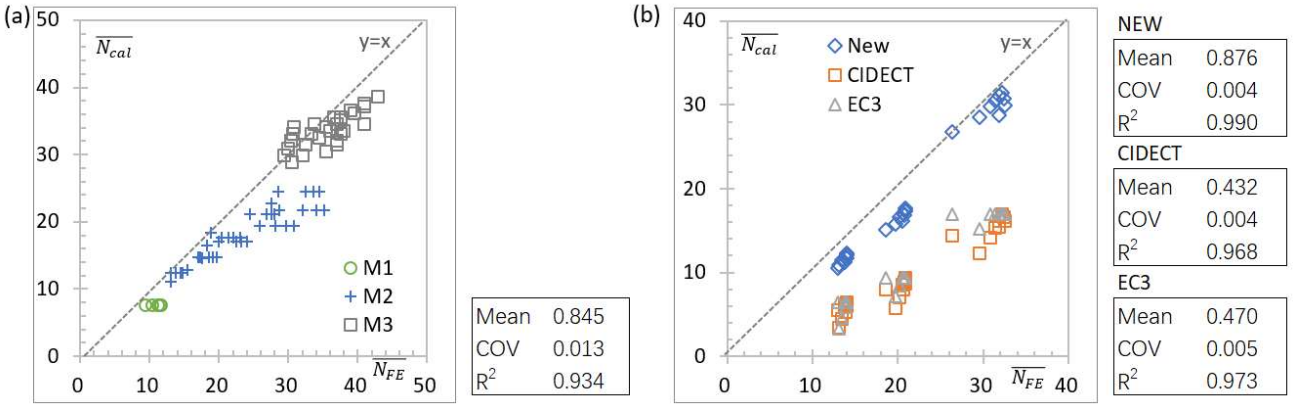

Fig. 17. Comparisons of the normalized strength between the equations and the FE analysis: (a). CPR T-joints without chord stress; (b). CPR T-joints with chord stress.

Failure mode of M1 can be excluded when the width of the collar plate being close to or equal to the flat width of the chord flange. Therefore, the failure modes M2 and M3 are more likely to occur and requires more attention for the compressive strength design of CPRT joints. In order to further verify the applicability of the new proposed equations, parameters of b_0, 2γ, β, γ_2 and τ_2 are expanded to carry out the L16-5-4 orthogonal analysis[2], as listed in Table 5. It is shown that the strength calculated by the proposed equations are around 85% of that of FE results, with the COV value of 0.009. Thus, the new proposed equations can be safely used for the design of CPR SHS T-joint. The predictions by Ozyurt[19] and Feng[20] are also included in Table 5 for comparison, the results by Feng[20] agree well with the FE data yet underestimate the strength for joints failure by M3, and the equations by Ozyurt[19] are over-conservative for most of the specimens.

Table 5 Comparison of new proposed equations and orthogonal parametric analysis results

Group	b_0	2γ	β	γ_2	τ_2	N_{FE}	N_{New}	N_{New} /N_{FE}	N_{Feng}	N_{Feng} /N_{FE}	N_{Ozyurt}	N_{Ozyurt} /N_{FE}	Failure Mode
O1	100	30	0.4	1	1	48.9	49.8	1.02	60.6	1.24	52.1	1.06	M2
O2	100	25	0.5	1.2	1.5	127.0	105.7	0.83	94.5	0.74	77.6	0.61	M2
O3	100	20	0.7	1.4	2	390.0	289.3	0.74	208.0	0.53	131.0	0.34	M3
O4	100	32.5	0.8	1.6	2.5	234.7	174.9	0.75	109.0	0.46	56.2	0.24	M3
O5	150	25	0.4	1.4	2.5	370.0	282.4	0.76	195.3	0.53	183.4	0.50	M2
O6	150	30	0.5	1.6	2	231.0	198.1	0.86	148.4	0.64	125.3	0.54	M2
O7	150	32.5	0.7	1	1.5	290.5	219.9	0.76	179.1	0.62	106.3	0.37	M2
O8	150	20	0.8	1.2	1	751.4	620.6	0.83	641.2	0.85	274.1	0.36	M3
O9	200	20	0.4	1.6	1.5	595.9	560.4	0.94	538.0	0.90	482.2	0.81	M2
O10	200	32.5	0.5	1.4	1	192.1	200.1	1.04	225.2	1.17	177.7	0.93	M2
O11	200	30	0.7	1.2	2.5	828.1	677.7	0.82	373.2	0.45	244.0	0.29	M3
O12	200	25	0.8	1	2	1059.5	861.1	0.81	733.3	0.69	357.1	0.34	M3
O13	250	32.5	0.4	1.4	2	488.7	397.9	0.81	323.4	0.66	293.4	0.60	M2

O14	250	20	0.5	1	2.5	1807.4	1444.6	0.80	916.3	0.51	808.2	0.45	M2
O15	250	25	0.7	1.6	1	1018.3	825.9	0.81	836.5	0.82	474.0	0.47	M2
O16	250	30	0.8	1.2	1.5	1054.2	1071.4	1.02	798.4	0.76	363.0	0.34	M3
Mean								0.850		0.724		0.515	
COV								0.009		0.051		0.053	

6. Conclusion

The compressive strength of CPR SHS T-joints was investigated by extensive parametric analysis, key parameters and typical failure modes were identified, and failure-mode-based design formulae were proposed. The following are major summaries:

(1) The current FE model results agree well with that of the experimental specimens in term of failure modes, load-displacement curves and the ultimate capacities, providing confident basis for the following parametric studies on CPR SHS T-joints.

(2) The geometrical parameters such as β, τ_2, η_2 and γ_2 show positive correlation with the compressive strength of CPR SHS T-joints, and the values of β and τ_2 are more influential and should be treated as the key parameters.

(3) Three failure modes are found to dominate for the compressive CPR T-joints, namely, chord flange yielding, chord flange and collar plate yielding, and chord web buckling. The change of the failure modes depends on the change of β, τ_2 and η_2.

(4) The presence of collar plate reinforcement tends to decrease the negative effects of chord stress ratio, and a new chord stress function is proposed for CPR joints, which agree well with the parametric data.

(5) The failure-mode-based design equations are more stable and accurate to predict the compressive strength of CPR SHS T-joints, which can provide reference for the practicing engineers.

Although the current study covers a practical variation of the dimensional parameters of the joints, the effect of chord stress ratio is preliminarily studied by applying axial load to the chord ends only. Noticed the chord stress ratio often refers to the total chord stress composed of the axial stress and the equilibrium induced stress in the chord, more experimental tests and FE simulations are needed to expand the applicability of current chord stress function.

Acknowledgments

The financial supports of the National Science Foundation of China (grant number 51978657) and the Fundamental Research Funds for the Central Universities (2018XKQYMS19), the Key R&D project of Xuzhou city (grant number KC19199) are greatly appreciated.

References

[1] J. Wardenier, Hollow sections in structural application, Second edition, Bouwen met Staal, Netherlands; 2011.

[2] H.F. Chang, W.K. Zuo, J.W. Xia, B. Xu, R.W. Ma, L.H. Zhang, Sensitivity analysis of geometrical design parameters on the compressive strength of the vertical inner-plate reinforced square hollow section T-joints: A finite element study, Engineering Structures. 208 (2020) 110308.

[3] H. Qu, J.S. Huo, C. Xu, F. Fu, Numerical studies on dynamic behavior of tubular T-joint subjected to impact loading. Int. J. Imp. Eng. 67 (2014) 12-26.

[4] J.W. Xia, H.F. Chang, M.G. Helen, Y.D. Bu, Y.M. Lu, Axial hysteretic behavior of doubler-plate reinforced square hollow section tubular T-joints, Mar. Struct. 55 (2017) 162-181.

[5] G.J. van der Vegte, Y.S. Choo, J.X. Liang, N. Zettlemoyer, J.Y.R. Liew, Static Strength of T-Joints Reinforced with

Doubler or Collar Plates. II: Numerical Simulations, J. Struct. Eng. 131(1) (2005) 129-138.

[6] C.Y. Wang, Y. Chen, X.X. Chen, D.F. Chen, Experimental and numerical research on out-of-plane flexural property of plates reinforced SHS X-joints, Thin-Walled Struct. 94 (2015) 466-477.

[7] L. Zhu, Q.M. Song, Y. Bai, Y. Wei, L.M. Ma, Capacity of steel CHS T-Joints strengthened with external stiffeners under axial compression, Thin-Walled Struct. 113 (2017) 39-46.

[8] W.P. Li, S.G. Zhang, W.Y. Huo, Y. Bai, L. Zhu, Axial compression capacity of steel CHS X-joints strengthened with external stiffeners, J. Constr. Steel Res. 141 (2018) 156-166.

[9] M. Lesani, M.R. Bahaari, M.M. Shokrieh, Experimental investigation of FRP-strengthened tubular T-joints under axial compressive loads, Constr. Build Mater. 53 (2014) 243-252.

[10] M. Lesani, M.R. Bahaari, M.M. Shokrieh, FRP wrapping for the rehabilitation of Circular Hollow Section (CHS) tubular steel connections, Thin-Walled Struct. 90 (2015) 216-234.

[11] X.X. Chen, Y. Chen, D.F. Chen, Plate reinforced square hollow section X-joints subjected to in-plane moment, J. Cent. South Univ. Technol. 22(3) (2015) 1002-1015.

[12] Y. Chen, D.F. Chen, Ultimate capacities formulae of collar and doubler plates reinforced SHS X-joints under in-plane bending, Thin-Walled Struct. 99 (2016) 21-34.

[13] N.V. Gomes, L.R.O. de Lima, P.C.G. Da S. Vellasco, A.T. Da Silva, M.C. Rodrigues, L.F. Costa-Neves, Experimental and numerical investigation of SHS truss T-joints reinforced with sidewall plates, Thin-Walled Struct. 145 (2019) 106404.

[14] H.F. Chang, W.K. Zuo, T.L. Ren, J.W. Xia, Z. Guo, Compressive behavior of plate-reinforced square hollow section T-joints. Journal of South China University of Technology (Natural Science Edition). 47(11) (2019) 113-121(in Chinese).

[15] H. Nassiraei, L. Zhu, M.A. Lotfollahi-Yaghin, H. Ahmadi, Static capacity of tubular X-joints reinforced with collar plate subjected to brace compression, Thin-Walled Struct. 119 (2017) 256-265.

[16] Y.S. Choo, G.J. van der Vegte, N. Zettlemoyer, B.H. Li, J.Y.R. Liew, Static Strength of T-Joints Reinforced with Doubler or Collar Plates. I: Experimental Investigations, J. Struct. Eng. 131(1) (2005) 119 -128.

[17] H. Nassiraei, M.A. Lotfollahi-Yaghin, H. Ahmadi, Static strength of collar plate reinforced tubular T/Y-joints under brace compressive loading, J. Constr. Steel Res. 119 (2016) 39-49.

[18] Y.B. Shao, Static strength of collar-plate reinforced tubular T-joints under axial loading, Steel Compos. Struct. 21(2) (2016) 323-342.

[19] E. Ozyurt, S. Das, Experimental and numerical studies on axially loaded reinforced square hollow section T-joints, Eng. Struct. 192 (2019) 323-334.

[20] R. Feng, Y. Chen, D.F. Chen, Experimental and numerical investigations on collar plate and doubler plate reinforced SHS T-joints under axial compression, Thin-Walled Struct. 110 (2017) 75-87.

[21] H.F. Chang, J.W. Xia, F.J. Zhang, Compression behavior of doubler-plate reinforced square hollow section t-joints, Adv. Steel Constr. 10 (2014) 289-309.

[22] L.R.O. de Lima, L.C.B. Guerrieiro, P.C.G. Da S. Vellasco, L.F. Costa-Neves, A.T. Da Silva, M.C. Rodrigues, Experimental and numerical assessment of flange plate reinforcements on square hollow section T joints, Thin-Walled Struct. 131 (2018) 595-605.

[23] EN 1993-1-8, Eurocode 3: Design of steel structures - Structures - Part 1-8: Design of joints. CEN, ECCS, Brussels, 2010.

[24] J.A. Packer, J. Wardenier, X.L. Zhao, G.J. van der Vegte, Y. Kurobane, Design guide for rectangular hollow section (RHS) joints under predominantly static loading, Comité International pour le Developpement et l'Etude de la Construction Tubulaire (CIDECT), Design Guide N.3, second ed., LSS Verlag, Dortmund, Germany, 2009.

[25] CECS 280:2010: Technical specification for structures for steel hollow sections. Beijing: China Planning Press, 2010

(in Chinese).

[26] D.K. Liu, J. Wardenier, G.J. van der Vegte. New chord stress functions for rectangular hollow section joints. The Fourteenth International Offshore and Polar Engineering Conference. Toulon, France: International Society of Offshore and Polar Engineers, 2004.

[27] M. Garifullin, M. Bronzova, S. Pajunen, K. Mela, M. Heinisuo, Initial axial stiffness of welded RHS T joints, J. Constr. Steel Res. 153 (2019) 459-472.

[28] H. Qu, A.L. Li, J.S. Huo, Y.Z. Liu, Dynamic performance of collar plate reinforced tubular T-joint with precompression chord, Eng. Struct. 141 (2017) 555-570.

[29] Y. Chen, Z.Z. Hu, Y. Guo, J.Y. Wang, G.S. Tong, Q.S. Liu, Y. Pan, Effects of chord pre-load on strength of CHS X-joints stiffened with external ring stiffeners and gusset plates, Eng. Struct. 195 (2019) 125-143.

[30] W.J. Wang, Y.B. Shao, H. Xia. Research on the static strength of square tubular T-joints reinforced with collar plate under axial compression reinforced with collar plate under axial compression. Engineering Mechanics. 29(6) (2011) 138-145 (in Chinese).

[31] H.F. Chang, J.W. Xia, Z. Guo, C. Hou, W. Din, F.Y. Qin, Experimental study on the axial compressive strength of vertical inner plate reinforced square hollow section T-joints, Eng. Struct. 172 (2018) 131-140.

[32] F. Gao, X.Q. Guan, H.P. Zhu, X.N. Liu, Fire resistance behaviour of tubular T-joints reinforced with collar plates, J. Constr. Steel Res. 115 (2015) 106-120.

[33] X.L. Zhao, J. Wardenier, J.A. Packer, G.J.V.D. Vegte, Current static design guidance for hollow-section joints, Proceedings of the Institution of Civil Engineers - Structures and Buildings. 163(6) (2010) 361-373.

[34] Y.S. Choo, X.D. Qian, J.Y.R. Liew, J. Wardenier, Static strength of thick-walled CHS X-joints-Part II. Effect of chord stresses, J. Constr. Steel Res. 59(10) (2003) 1229-1250.